

1 **Reply to the Review Comments #1 and #2**

2

3 **Contents**

4

5 **Section 1. Reply to the Review Comments #1.**

6

7 **Section 2. Reply to the Review Comments #2.**

8

9 **Section 3. Marked-up manuscript. Pages 1-28.**

10

11 Note: The **bolded Page Numbers** in Replies of Section 1&2 refer to page numbers of
12 Section 3

13

Section 1. Reply to the Review Comments #1

Reply to the Review Comments #1

1
2
3 Thank you for your substantial and detailed comments! According to these comments, we revised
4 the manuscripts and gave our replies to these comments point by point. The original manuscript,
5 the revised version and the added references are listed if necessary. The **yellow highlights** mark
6 the revised parts and the new references according to the Review Comments #1.

7
8 Note that this reply is focusing on the Review Comments #1. The revised parts and the new
9 references according to the Review Comments #2 are marked with **red colors** when there are
10 overlaps.

Major comments:

11
12
13 **The current manuscript presents a detailed analysis of large scale travelling ionospheric**
14 **disturbances which occurred during the March 17, 2015 geomagnetic storm. The**
15 **authors combined data from multiple GNSS receiver networks to create 2-dimensional**
16 **maps of total electron content perturbations from where azimuth, velocity and periods**
17 **were determined. In addition, they made use of ionosondes and HF doppler radars, and**
18 **in my view, have presented a very complete and comprehensive study especially**
19 **focusing on the northern hemisphere mid-latitude region over the Asian region. They**
20 **intentionally avoided discussing low latitude changes or TID related variations in this**
21 **particular region (which I think they shouldn't have) as I will point out later in the**
22 **comments. Nevertheless, this is an important contribution to the TIDs studies. In my**
23 **view, the strength of this paper is two-fold**

- 24 **1. The utilization of dense networks of diverse instrumentation (GNSS receivers, doppler**
25 **radars and ionosondes) to bring out finer details of large scale TIDs during the March**
26 **17, 2015 geomagnetic storm.**
- 27 **2. The agreement of TID velocity estimated from 2-D TEC perturbation maps and HF**
28 **doppler radar data. In fact the authors missed an opportunity to discuss this issue in**
29 **detail and should be revised in the paper as it is an interesting one. Let me elaborate in**
30 **more details here. From their Figure 3, they estimated the TID velocity to be 553 m/s**
31 **(between 10:24-10:45 UT). Later in Figure 8, the estimated velocity from VTECP' maps**
32 **(I assume it to be around the same time because the time of V_t and V_c was not actually**
33 **clearly stated) was 578 ± 16 m/s. Page 7, lines 36-37, they did comment that that '... V_t is in**
34 **good agreement with the result of 553 m/s derived from the Doppler observation'.**
35 **Usually velocity values estimated from spaced instruments such as ionosondes and HF**
36 **Doppler radars tend to be higher than the actual TIDs' velocities because it assumes**
37 **"perfect equatorward propagation". If the spaced instruments (e.g., ionosondes or**
38 **doppler radars are in 'perfect alignment' with the propagation of TIDs, then the**
39 **velocities from the two methods can have a high degree of agreement. Taking a look at**
40 **Figure 9 of the authors, their azimuth values point to this direction that the position of**
41 **the HF Doppler radars actually was in the direction of the TID's propagation. This may**
42 **be the main reason why the velocity values from these two methods agree. I encourage**

Section 1. Reply to the Review Comments #1

1 the authors to add some discussion in this regard. Below are the references that talk
2 directly to this second point

- 3 • Afraimovich et al., (1998), GPS radio interferometry of travelling ionospheric disturbances,
4 J. Atmos. Solar. Terr. Phys., 60, 1205-1223
- 5 • Habarulema et al., (2013), Estimating the propagation characteristics of large-scale
6 traveling ionospheric disturbances using ground-based and satellite data, J. Geophys.
7 Res. Space Physics, 118, 7768-7782, doi:10.1002/2013JA018997

9 Reply to Major Comment:

10 Thanks for your evaluation of this manuscript and good suggestions. Based on your suggestion,
11 we try to add some discussions about the result of HF Doppler and VTECP'. Considering this
12 suggestion and the detail comments, the following paragraph about the relationship of the velocity
13 of LSTID derived from HF Doppler and VTECP' is added in the revised manuscript.

14
15 **Page 8, Lines 34-43; Page 9, Line 1:**“In addition, it is interesting to note that V_t is in reasonable
16 agreement with the result of 535 m/s derived from the Doppler recordings. To show it more
17 specifically, we estimated the speed and direction of the LSTID using the same TLP method as
18 Figure 8 but in 111°E-114°E and 29°N-38°N (corresponding to the reflecting points). The result is
19 562 ± 59 m/s and 0°, respectively. In general, the LSTID velocity estimated from ground-based
20 stations tend to be larger than the actual velocity since these stations, in most cases, are not in
21 perfect alignment with the propagation direction of the LSTID [Afraimovich et al., 1998;
22 Habarulema et al., 2013]. Such good agreement between VTECP' and HF Doppler results may be
23 attributed to the fact that the reflecting points (29.2°N,111.8°E; 38.0°N,113.2°E) of the Doppler
24 receivers are in a narrow longitudinal band and the direction of the LSTID's propagation is also
25 almost due south between 111°E-114°E.”

28 Detail comments

29 Abstract:

30 **Comment 1**

31 Page 1, lines 13-15 which talk about first observation of LSTIDs in East Asian sector for the first
32 time may not necessarily be entirely correct. I would like to point the authors to Habarulema et al.,
33 (2018) which analysed LSTIDs during this storm period in the African, Asian and American
34 regions. These authors reported LSTIDs in the Asian region between 0900-1200 UT reaching
35 velocity values of over 800 m/s. Perhaps in the current paper, the authors have used more data and
36 so their propagation parameters maybe 'more accurate', but certainly this is not the first study over
37 the Asian sector for this particular storm. Please re-word this accordingly.

38 Reference: Habarulema et al., (2018): Storm time global observations of large-scale TIDs from
39 ground-based and in situ satellite measurements. Journal of Geophysical Research: Space Physics,
40 123, 711-724, <https://doi.org/10.1002/2017JA024510>.

Section 1. Reply to the Review Comments #1

Reply 1

Thanks for pointing it out. We missed this reference and made the inappropriate statement of the “first observation”. According to this comment, the manuscript is revised. The reference “Habarulema et al., (2018)” is added in the reference list, and necessary discussions are also given in the revised manuscript (e.g., Revision 3, 17).

The statements in the original manuscript

“This study gives the first observation of the large-scale traveling ionospheric disturbances (LSTIDs) in the East Asian sector during the 2015 St. Patrick’s Day (March 17, 2015) geomagnetic storm.

...

Using data from 4 GPS receiver networks (CMGN, CMONOC, GEONET, IGS), together with recordings of 2 HF Doppler shift stations and 8 ionosondes, we show the first observation results of the LSTIDs in the East Asian sector during the 2015 St. Patrick’s Day storm.”

are revised as:

Page 1, Lines 10-12: “This study presents a comprehensive observation of the large-scale traveling ionospheric disturbances (LSTIDs) in the East Asian sector during the 2015 St. Patrick’s Day (March 17, 2015) geomagnetic storm.”

...

Page 11, lines 25-28: “Using data from 4 GPS receiver networks (CMGN, CMONOC, GEONET, IGS), together with recordings of 2 HF Doppler shift stations and 8 ionosondes, we provide comprehensive and detailed observation results of the LSTIDs in the East Asian sector during the 2015 St. Patrick’s Day storm.”

Added Reference

Page 14, lines 27-29: Habarulema, J. B., Yizengaw, E., Katamzi-Joseph, Z. T., Moldwin, M. B., and Buchert, S.: Storm Time Global Observations of Large-Scale TIDs From Ground-Based and In Situ Satellite Measurements. *Journal of Geophysical Research: Space Physics*, 123(1), 711-724, 2018.

Comment 2

Page 1, lines 17-19, the concept of negative and positive LSTID is not understandable. Usually TIDs are seen as periodic changes in VTECP or electron density appearing like wave structures. As such, these structures would have ‘troughs’ and ‘crests’. What are the authors calling negative LSTIDs? Is it where VTECP is negative? Shouldn’t this be the ‘troughs’ of the wave or TID? Please check this and revise if necessary.

Reply 2

Very thanks! According to this comment, the some statements in the original manuscript are revised.

“Results show that a negative LSTID spanning at least 60° in longitude (80°E-140°E) occurs and propagating from high to lower latitudes around 09:40-11:20 UT. It is followed by a positive LSTID which shows a tendency of dissipation starting from the East side.”

is revised as:

Section 1. Reply to the Review Comments #1

1 **Page 1, Lines 14-17:** “Results show that a trough of LSTID spanning at least 60° in
2 longitude (80°E-140°E) occurs and propagates from high to lower latitudes around 09:40-11:20
3 UT. It is followed by a crest of LSTID which shows a tendency of dissipation starting from the
4 East side.”

5
6 “(1) A negative LSTID occurs and propagates from high to lower latitudes during
7 09:40-11:20 UT, which spans over 60° in longitude. It is followed by a positive LSTID
8 characterized by a clear tendency to dissipate which starts from the East side.”

9 is revised as:

10 **Page 11, lines 33-35:** “(1) A trough of LSTID occurs and propagates from high to lower
11 latitudes during 09:40-11:20 UT, which spans over 60° in longitude. It is followed by a crest of
12 LSTID that characterized by a clear tendency to dissipate starting from the East side.”

13 14 **Introduction:**

15 16 **Comment 3**

17 Page 2, lines 4-6, perhaps, the authors can talk about AGWs in general as they can also lead
18 to MSTIDs? I think in the introduction, the authors missed critical papers which have done similar
19 analysis for the March 17, 2015 storm. They include: Borries et al., (2016): Multiple ionospheric
20 perturbations during the Saint Patrick’s Day storm 2015 in the European-African sector. Journal of
21 Geophysical Research: Space Physics, 121, 11333-11345, <https://doi.org/10.1002/2016JA023178>;
22 and Ramsingh et al., (2016): Low-latitude ionosphere response to super geomagnetic storm of
23 17/18 March 2015: Results from a chain of ground-based observations over Indian sector. Journal
24 of Geophysical Research: Space Physics, 120, 10864-10882,
25 <https://doi.org/10.1002/2015JA021509>

26 **Reply 3**

27 According to this comment, the first paragraph is rewritten and some references are cited in
28 suitable place in the revised manuscript.

29 **The first and last paragraphs of Introduction**

30 “In general, the response of the ionosphere to the geomagnetic storm is classified by a variety
31 of different features, one of which is the large scale traveling ionospheric disturbance (LSTID). It
32 is the wave-like perturbation mainly propagating equatorward from high latitudes that is
33 considered to be the manifestation of the presence of atmospheric gravity waves (AGWs) within
34 the ionosphere caused by Joule heating or Lorenz-drag forcing in the Auroral regions during
35 geomagnetic storm period [Hines, 1960; Richmond and Roble, 1979; Hocke and Schlegel, 1996].

36

37 During the period of 17–18, March 2015, a large geomagnetic storm occurred, which is the
38 strongest one in the 24th solar cycle. During this storm, LSTIDs over European and American
39 sectors are detected and analyzed with data from Global Navigation Satellite Systems (GNSS)
40 stations [Zakharenkova et al., 2016]. Meanwhile, two high frequency (HF) Doppler stations
41 operated by China Meridional Project [Wang, 2010] at mid-latitude China record a large
42 ionospheric HF Doppler shift after 10:00 UT, which appears to indicate LSTIDs related to the
43 geomagnetic storm. In this study, the multi-network of densely distributed GPS receivers and an

Section 1. Reply to the Review Comments #1

1 ionosonde network will be used to reveal the propagating characteristics of these large
2 disturbances recorded in HF Doppler shift receivers in the East Asian region, especially the
3 characteristics of the dominant propagating direction of this disturbance over China and Japan.”

4
5 are revised as:

6 **Page 2, lines 4-12:** “In general, the response of the ionosphere to the geomagnetic storm is
7 classified by a variety of different features, one of which is the large scale traveling ionospheric
8 disturbance (LSTID) that is the wave-like perturbation mainly propagating equatorward from high
9 latitudes. Traveling ionospheric disturbances (TIDs) are classified into LSTIDs and Medium-scale
10 TIDs and they are considered to be the ionospheric manifestation of the presence of atmospheric
11 gravity waves (AGWs) stimulated by different sources. LSTIDs are mainly caused by Joule
12 heating or Lorenz-drag forcing in the Auroral regions during geomagnetic storm period [Hines,
13 1960; Richmond and Roble, 1979; Hocke and Schlegel, 1996].”

14

15 **Page 3, lines 24-44:** “During the period of 17–18, March 2015, the strongest geomagnetic
16 storm in the 24th solar cycle occurred and LSTIDs are detected and analysed in different
17 longitudinal sectors [Ramsingh et al., 2015; Borries et al., 2016; Zakharenkova et al., 2016;
18 Habarulema et al, 2018]. Meanwhile, two high frequency (HF) Doppler stations operated by China
19 Meridional Project [Wang, 2010] at mid-latitude China record large ionospheric HF Doppler shifts
20 after 10:00 UT, which seem to indicate the LSTIDs in the Asian region between 09:00-12:00 UT
21 that reported by Habarulema et al. [2018]. In this study, the multi-network of densely distributed
22 GPS receivers, the HF Doppler stations, and an ionosonde network are used to conduct a more
23 comprehensive study on the propagating characteristics of the disturbances in the East Asian
24 region, especially on the characteristics of the dominant propagating direction over China and
25 Japan.”

26
27 **Following References are added in the reference list**

28 **Page 13, lines 16-18:** Borries, C., Mahrous, A. M., Ellahouny, N. M., and Badeke, R.: Multiple
29 ionospheric perturbations during the Saint Patrick's Day storm 2015 in the European-African
30 sector. *Journal of Geophysical Research: Space Physics*, 121(11), 11-333, 2016.

31 **Page 15, lines 32-35:** Ramsingh, Sripathi, S., Sreekumar, S., Banola, S., Emperumal, K., Tiwari,
32 P., and Kumar, B. S.: Low-latitude ionosphere response to super geomagnetic storm of 17/18
33 March 2015: Results from a chain of ground-based observations over Indian sector. *Journal*
34 *of Geophysical Research: Space Physics*, 120(12), 10-864, 2015.

36 **Data and Methods:**

37 **Comment 4**

38
39 Page 4, lines 36-39 which discuss the ionosonde data that have been used in the study. Has
40 this data been manually cross-checked to ensure that erroneous ionograms were not used in the
41 analysis and interpretation? This may be one of the errors associated with Figure 6 where the
42 downward phase propagation did not manifest in a number of stations? I will comment on this
43 later. For some reference about errors that could be in data due to wrongly scaling of ionograms,

Section 1. Reply to the Review Comments #1

1 please see Habarulema and Carelse (2016), I think their Figure 1?: Long-term analysis between
2 radio occultation and ionosonde peak electron density and height during geomagnetic storms,
3 Geophys. Res. Lett., 43, 4106-4111, doi:10.1002/2016GL068944; and Krankowski et al., (2011),
4 Figures 4-5 : Ionospheric electron density observed by FORMOSAT-3/COSMIC over the
5 European region and validated by ionosonde data, J. Geod., 85, 949-964

6 7 **Reply 4**

8 Thank you for raising concerns about the error checking.

9 The virtual height data in Figure 6 is manually scaled by ourselves from ionograms with
10 professional scaling software provided by the China Research Institute of Radio wave Propagation
11 (CRIRP). The validity of these ionograms is supported by this institute and our manually scaling
12 has been checked by ourselves for a few times. We will make this clear in the revision.

13 We tend to believe that the data is not wrong. But as the reviewer mentioned, the downward
14 phase propagation is not clear in a number of stations. We think this may be attributed to the
15 relatively low temporal resolution of 15 minutes.

16
17 **According to this comment, we revised the statement**“In this study, ionograms from 8
18 ionosonde stations in China middle latitude are used to derive the iso-frequency lines, which vary
19 as a function of universal time and virtual height. The sample rate of the ionograms is 15 minutes.
20 These ionosondes belong to the China Research Institute of Radio-wave Propagation (CRIRP) and
21 their locations are marked in Figure 1 with lime triangles. In addition, the condition of the
22 geomagnetic storm is shown with data from the high resolution (5 minutes) OMNI dataset, which
23 is downloaded from the FTP service of the NASA Goddard Space Flight Center
24 (<https://spdf.gsfc.nasa.gov>).” as

25
26 **Page 4, Line 39 ~ Page 5, Lines 1-9:** “In this study, ionograms from 8 ionosonde stations in
27 China middle latitude are used to derive the iso-frequency lines, which vary as a function of
28 universal time and virtual height. The sample rate of the ionograms is 15 minutes. These
29 ionosondes belong to the China Research Institute of Radio-wave Propagation (CRIRP) and their
30 locations are marked in Figure 1 with green triangles. The virtual height data is manually scaled
31 by ourselves to reduce possible errors of auto scaling [Krankowski et al., 2011; Habarulema and
32 Carelse, 2016] from these ionograms with professional scaling software provided by CRIRP.
33 During the scaling, we limited the frequency to be less than 7 MHz. In addition, the condition of
34 the geomagnetic storm is shown with data from the high resolution (5 minutes) OMNI dataset,
35 which is downloaded from the FTP service of the NASA Goddard Space Flight Center.”

36
37 **And the two references are added in the reference list.**

38 **Page 14, Lines 18-20:** Habarulema, J. B. and Carelse, S. A.: Long-term analysis between radio
39 occultation and ionosonde peak electron density and height during geomagnetic storms.
40 Geophysical Research Letters, 43(9), 4106-4111, 2016.

41 **Page 15, Lines 6-8:** Krankowski, A., Zakharenkova, I., Krypiak-Gregorczyk, A., Shagimuratov, I.
42 I., and Wielgosz, P.: Ionospheric electron density observed by FORMOSAT-3/COSMIC over
43 the European region and validated by ionosonde data. Journal of Geodesy, 85(12), 949-964,
44 2011.

Section 1. Reply to the Review Comments #1

1

Observations:

2

3

Comment 5

4

Page 5, lines 20-21, the text sounds misleading. The reader may go to Figure 1 looking for the ‘disturbances which are observed successively’ only to find the location of HF doppler radars.

7

Reply 5

8

Thank you for pointing it. The misleading expression “During the first stage of the main phase, disturbances are observed successively at two HF Doppler receiver stations shown in Figure 1”

10

11

is revised as:

12

13

Page 5, Lines 30-31: “During the first stage of the main phase, disturbances are observed successively at MDT and SZT Doppler receiver stations.”

15

16

17

Comment 6

18

Page 5, Line 23, the times indicated here are different from the times shown by arrows in Figure 3 of 10:24 UT and 10:45 UT?

20

21

Reply 6

22

Thank you for pointing out this discrepancy. After checking the data we find that the occurrence time of the positive shifts are about 10:22 UT and 10:53 UT. The speed estimated from HF Doppler is about 535 m/s.

25

26

According to this, figure 3 is redrawn and the statement

27

“It shows that two distinct positive shifts occur at about 10:21 UT and 10:55 UT, respectively. ... the approximate speed of this perturbation is about 533 m/s.”

28

29

is revised as:

30

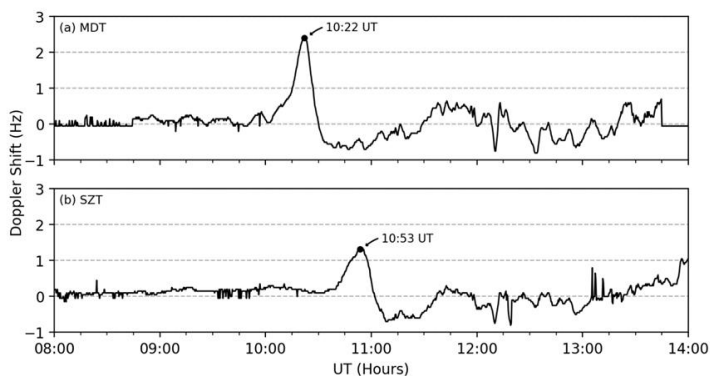
Page 5, Lines 32-33, 36-37: “It shows that two distinct positive shifts occur at about 10:22 UT and 10:53 UT, respectively. ... the approximate speed of this perturbation is about 535 m/s.”

32

33

Revised figure 3

34



35

Section 1. Reply to the Review Comments #1

1
2
3
4
5
6
7
8
9
10
11
12
13
14
15
16
17
18
19
20
21
22
23
24
25
26
27
28
29
30
31
32
33
34
35
36
37
38
39
40
41
42
43
44

Comment 7

Page 5, Lines 30-32, the authors should mention the limitation of this assumption to be valid when the AGW is in a perfectly equatorward direction and add references I mentioned in the opening statements

Reply 7

Thank you for the thought-provoking suggestion.

With this sentence, we just want to give a rough classification of the disturbances based on the magnitude of the estimated speed. The detail illustration and velocity estimation will be given in the following text with VTECP method. We have revised the text to make it clear.

Please refer to Reply 16 for detail. The references are also added in Revision 16.

The sentence in the original manuscript “Considering the propagating speed and the interval of the positive-negative variations, the recorded perturbations probably reflect an equatorward propagating LSTID in the East Asian sector.”

is revised as:

Page 5, lines 40-42: “Considering the magnitude of the speed and the time interval of the positive-negative variations, the recorded perturbations probably reflect an equatorward propagating LSTID in the East Asian sector.”

Comment 8

Page 5, Lines 33-34 are not clear. If the authors refer to the equation in section 2, then perhaps number it and refer to it here. Otherwise ‘above’ doesn’t give appropriate guidance to the reader.

Reply 8

Thank you very much!

With “above” we want to refer to the VTECP map method described in section 2 in the paragraph that includes the equations but not just the equations. As the comment describes, just say “above” is inappropriate indeed and it is reworded to “in section 2”. The equations are also numbered.

According to this comment, the sentence is revised as:

Page 6, lines 1-2: “To confirm this, Figure 4 presents a sequence of 2D VTECP maps between 09:40-11:40 UT on 17 March 2015 with the method described in section 2.”

Comment 9

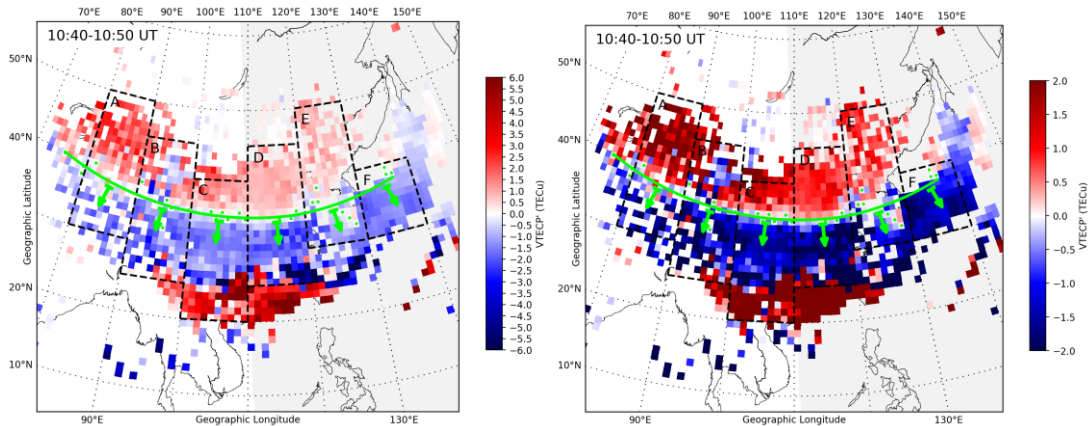
The motivation of transforming VTECP to VTECP’ is not very clear to me. If the method used to estimate the background TEC values is consistently used, why would this be required? May be the VTECP values will be significantly small, but positive and negative perturbations should still come out of the 2-D maps?

Reply 9

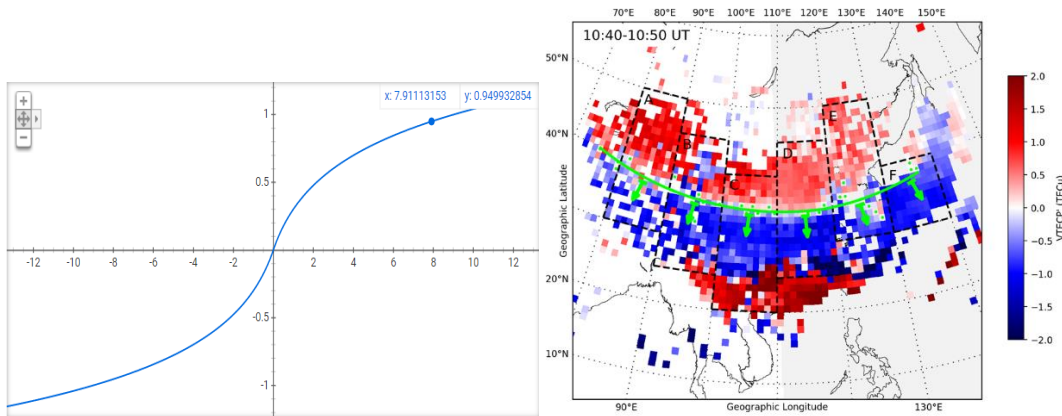
Thank you very much for pointing out the confusing expression.

Section 1. Reply to the Review Comments #1

1 In short, this transformation is not absolutely necessary but it will make the colormap of the
 2 2D VTECP plots looks better. Below is the original 2D VTECP map without the transform.



3
 4 The fact is that the perturbations in the EIA region is much larger than that in the mid
 5 latitudes. If we choose a colormap based on the values of the lower latitudes, the color in the mid
 6 latitudes will be too light (left figure). If we choose a colormap based on the values of the mid
 7 latitudes, the color in the lower latitude will be too dark and lose details (right figure).



8
 9 The left is the plot of the transform equation $y = \text{sgn}(x) * \log_{10}(\text{abs}(x) + 1)$. It
 10 accelerates the changes when x approaches 0 and decelerates the changes when x deviates 0. So
 11 with this transform, we can sharpen the edges between positive and negative values and reduce the
 12 differences of large and small absolute values. The outcome is the right figure.

13 We have revised the text to make this clear.

14 **The original description**

15 “Note that the raw value of VTECP is converted into VTECP’ with

16
$$\text{VTECP}' = \text{sign}(\text{VTECP}) * \log_{10}(\text{abs}(\text{VTECP}) + 1)$$

17 to make it easier to distinguish the regions with positive and negative perturbations.”

18 **is revised as:**

19 **Page 6, Lines 2-7:** “The raw value of VTECP has already been converted into VTECP’ with
 20 the equation

21
$$\text{VTECP}' = \text{sgn}(\text{VTECP}) * \log_{10}(\text{abs}(\text{VTECP}) + 1) \quad (3)$$

22 The raw amplitude of VTECP above 30°N is ~ 2 TECu while the raw amplitude of VTECP below
 30°N reaches ~ 10 TECu. So, transform (3) provides a better colormap for 2D VTECP plots by

Section 1. Reply to the Review Comments #1

1 sharpening the edges between positive and negative values and reduce the differences of VTECP
2 in middle and low latitudes.”

3 4 5 **Comment 10**

6 Page 5, Line 39 and everywhere, Lime lines appear green? Not sure of the color. The issue
7 which requires more details is where the authors talk about ‘values close to zero’. How close to
8 zero? Is it possible to provide a range may be between -0.05 and 0.05?

9 **Reply 10**

10 Thank you very much for pointing out the confusing parts.

11 To reduce confusion, **the word “lime” is replaced with “green”** in the revised manuscript.

12 The criterion of “close to zero” is a little confusing indeed. In short, we selected the bottom 5%
13 absolute VTECP’ values in selected areas according to different plots. We had planned to give a
14 detailed interpretation in section 3.2 with Figure 7 so we just gave a guidance of “see below for
15 example”. We have revised the text to make it clear.

16
17 According to this comment, the sentence

18 “The lime lines are similar but for pixels with values close to zero (see below for example)”
19 **is revised as**

20 **Page 6, Lines 10-11:** “The green lines are similar but for pixels with the bottom 5% absolute
21 VTECP’ values in selected areas (see section 3.2 for a detailed example).”

22 23 24 **Comment 11**

25 Page 6, Lines 10-17, I suggest that the author have a look at the paper by Pradipta et al.,
26 (2016): Interhemispheric propagation and interactions of auroral traveling ionospheric
27 disturbances near the equator. Journal of Geophysical Research: Space Physics, 121, 2462-2474,
28 <https://doi.org/10.1002/2015JA022043>

29 **Reply 11**

30 Thanks for recommending this paper. We revised the statements and added some contents
31 about the interhemispheric propagation of traveling ionospheric disturbances near the equator.
32 **More detail discussions can be seen in Reply to Comment 17.**

33
34 **Statements below are added.**

35 **Page 6, lines 32-35:** “Besides, Pradipta et al. [2016] studied the interaction of the auroral
36 LSTIDs from opposite hemispheres near the dip equator during the 26 September 2011
37 geomagnetic storm. It shows that such interaction may bring much complexity to the TEC
38 perturbations near the dip equator.”

39
40 **Added Reference**

41 **Page 15, lines 29-31:** “Pradipta, R., Valladares, C. E., Carter, B. A., and Doherty, P. H.:
42 Interhemispheric propagation and interactions of auroral traveling ionospheric disturbances
43 near the equator. Journal of Geophysical Research: Space Physics, 121(3), 2462-2474, 2016.”

44

Section 1. Reply to the Review Comments #1

Comment 12

Page 6, Lines 18-27, considering Figure 5 where there is a temporal shift seen at 38 degrees North followed by 29 degrees North, have the authors considered investigating such LSTID to be originating from northern hemisphere and propagation towards the equator with possibility of crossing the equator towards the southern hemisphere?

Reply 12

Thank you for this suggestion.

Yes, we did have considered it. We have plotted TLPs like those in Figure 8 for different longitudinal bands with spatiotemporal ranges of 07:00-14:00 UT and 15°S-45°N. It can be seen that there seems to be propagating perturbations that cross the dip equator.

However, we decided not to include these rough results in our manuscript for two main reasons. On the one hand, our current work mainly focuses on the northern hemisphere mid latitude. The perturbations in the low latitude are related to various mechanisms and thus much complex. We may investigate perturbations in this region in our future works. On the other hand, the collected TEC data has a relatively low spatiotemporal coverage in the low latitude and southern hemisphere of this longitudinal sector during this storm period.

Comment 13

Page 6, lines 28-44, In my view, ionosonde data and its interpretation should be given more attention than is done in the current version. If the uplift of virtual height (h') is due to the AGW which results into the TID that reaches ionospheric heights, then we would have seen the dominant trend in downward phase velocity. An important consideration with ionosonde data is to check that scaling was done correctly as I have already mentioned. In the current manuscript, the authors paid too much attention to the higher iso-line and connected it to the one at the lower h' . In my opinion, this should be re-looked at, because the ionosonde is 'more accurate' at measuring the bottom-side ionosphere. Although I don't know the actual height corresponding to virtual height of 600 km, it may be possible that this could fall within the extrapolated topside? Therefore, in actual sense, we should be able to see the downward phase velocities from the lower h' values for the analysis to be reliable. For a recent analysis of ionosonde data during this storm period, please see <https://doi.org/10.1002/2017JA024510>.

Reply 13

Thanks for the suggestions about the ionosonde data.

This comment is related to the Comment 4 about the error checking. The virtual heights of the iso-frequencies were scaled from the consecutive ionograms with 15-minute sample rate. All the virtual heights are below the virtual height of the $h'F_2$. In order to obtain more useful data, the virtual heights near the peak F2 layer were also scaled and given in the original manuscript. The data scaling is done by ourselves with the professional scaling software provided by CRIRP. During the revision, we have checked this process again and thus we tend to believe that the data is credible. But as the reviewer point out, the trend in downward phase velocity is sometime not clear. We think this may be attributed to the low temporal resolution of 15 minutes.

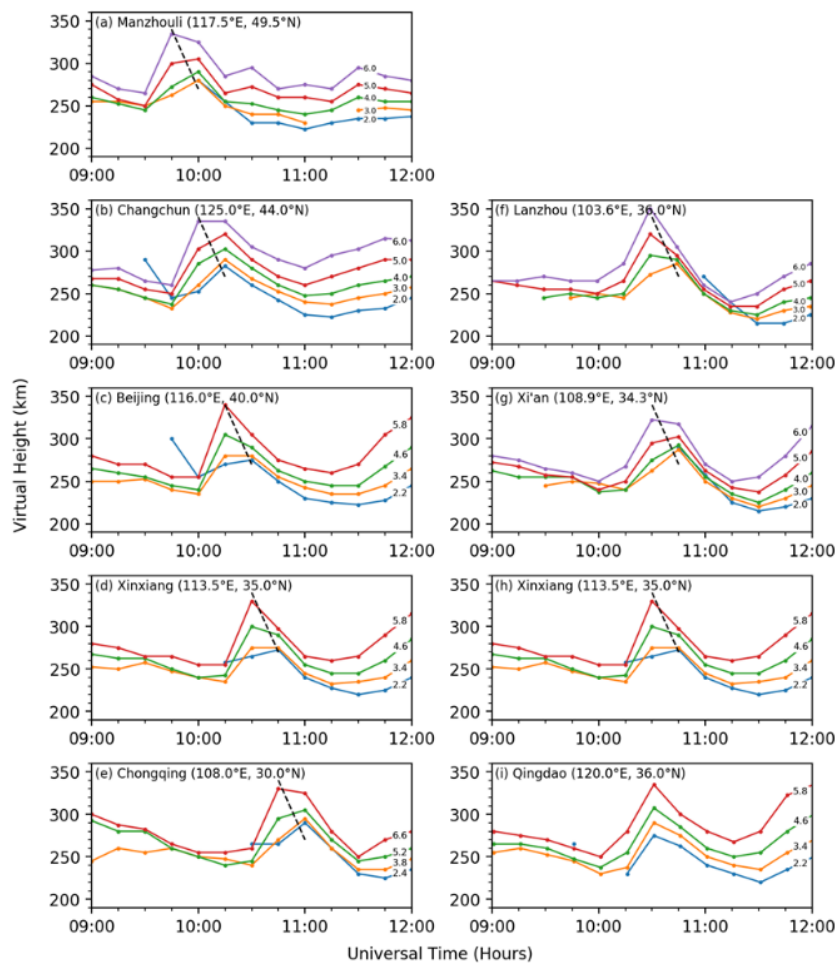
Another issue that the reviewer put forward is that we might pay too much attention to the

Section 1. Reply to the Review Comments #1

1 higher iso-line and the ionosonde is “more accurate” at measuring the bottom-side ionosphere. We
2 check the iso-frequency lines and find that just as the reviewer point out, the downward phase
3 velocity, if it can be detected in a ionosonde station, mainly occurs in lower h' (frequency). So
4 considering this fact, we revise the iso-frequency plots by limiting the frequency to be less than 7
5 MHz. The text is also revised accordingly.

6
7 **The revised content about this paragraph and the revised figure is as follows:**

8
9 **Page 7, lines 6-24:** “Ionospheric parameters from ionograms have been commonly used
10 since early TID studies. Recently, ionograms and iso-frequency lines with different sampling rates
11 were used in TID studies [Klausner et al, 2009; Ding et al., 2012, 2013; Pradipta et al., 2015;
12 Ramsingh et al., 2015; Habarulema et al., 2018]. Figure 6 presents the temporal variations of the
13 virtual height for each iso-frequency line. The names and locations of the corresponding
14 ionosondes are given in each subplot as annotates. The sampling frequency are marked on the
15 right side for each line. On the left column, the results of five stations are arranged in order from
16 high to lower latitudes, and on the right column, it shows the recordings of four stations in the
17 same latitudinal belt. Such trends (marked with black dashed lines) indicate a downward
18 vertical phase velocity, which is one of the typical characteristics of TID and AGW [Hine, 1960;
19 Hocke and Schlegel, 1996]. It should be noted that the downward trend is not much clear for
20 certain station, especially the one in Qingdao. This may be attributed to the 15 minutes sampling
21 interval.”



Section 1. Reply to the Review Comments #1

1

2

3

Comment 14

4

Page 7, lines 11-12, the text which talks about morphology changes of the TID changing as it propagates from high to lower latitudes: Is this backed by any references? Because the analysis of the authors is limited to northern hemisphere mid-latitudes

5

6

Reply 14

7

Thank you very much.

8

The sentence in the original manuscript can be misunderstood. Here with this expression we just want to mention the TID morphology changes with time that shown in Figure 4. In the revised manuscript, we try to make this clearly as follows: .

9

10

11

Page 7, lines 35-36: “It should be noted that the morphology of this TID is continuously changing as it moves from high to lower latitudes in the studied region.”

12

13

14

15

16

Comment 15

17

Page 7, lines 15-20: The authors can consider labelling the 'rectangles' as A, B, C, etc or something along this line for the reader to easily identify them in the Figure.

18

19

Reply 15

20

Thanks for this suggestion. The labels are added and the text is revised accordingly as follows:

21

22

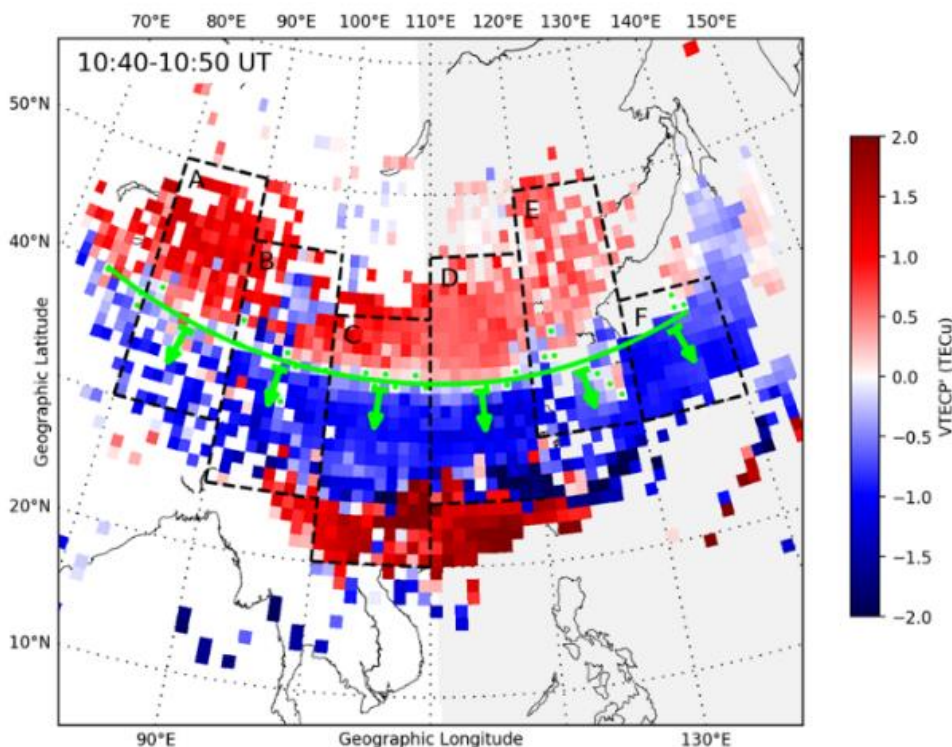
Page 7, Lines 41-42 ~ Page 8, Lines 1-2: “..., which are marked with dashed rectangles A-F in Figure 7. For each band, the VTECP' data is averaged along the latitude for every 6 minutes (0.1 hours), and the results as a function of UT and latitude are illustrated correspondingly in Figure 8 (a-f).”

23

24

25

26



27

Section 1. Reply to the Review Comments #1

Comment 16

Page 7, lines 37-38: This is where a discussion/description of the agreement between the two techniques (VTECP' and doppler radar) should have discussed. Please refer to my earlier comment in the opening statements.

Reply 16

Thanks for this thought-provoking suggestion.

Based on this comment and the Comment 7, we have revised the estimated speed (535 m/s) from Doppler recordings. To show the good agreement between this speed and the VTECP speed, we made a estimation of the VTECP speed specifically for the reflecting points' longitudinal band (111°E-114°E, 29°N-38°N). Related discussions have been added as a separate paragraph.

The original statement:

“It shows that V_t is in good agreement with the result of 553 m/s derived from the Doppler observation. These parameters are typical for an LSTID. Besides, it is interesting to note that the mean V_c is slightly larger than the mean V_t , which seems like the wave behind is pushing that ahead.”

is revised as:

Page 8, Lines 28-43 ~ Page 9, Line 1: “These parameters are typical for an LSTID. V_t and V_c overlap, although only marginally, considering the error ranges. Meanwhile, the mean V_c is slightly larger than the mean V_t , which seems like the wave behind is pushing that ahead. In general, the speed of trough and crest of the LSTID should be rather the same since they are induced by the same gravity wave. However, the wave properties might change with time dependent on the forcing from background condition, especially for LSTID covering large spatial region. This might explain the differences.

In addition, it is interesting to note that V_t is in reasonable agreement with the result of 535 m/s derived from the Doppler recordings. To show it more specifically, we estimated the speed and direction of the LSTID using the same TLP method as Figure 8 but in 111°E-114°E and 29°N-38°N (corresponding to the reflecting points). The result is 562 ± 59 m/s and 0° , respectively. In general, the LSTID velocity estimated from ground-based stations tend to be larger than the actual velocity since these stations, in most cases, are not in perfect alignment with the propagation direction of the LSTID [Afraimovich et al., 1998; Habarulema et al., 2013]. Such good agreement between VTECP' and HF Doppler results may be attributed to the fact that the reflecting points (29.2°N, 111.8°E; 38.0°N, 113.2°E) of the Doppler receivers are in a narrow longitudinal band and the direction of the LSTID's propagation is also almost due south between 111°E-114°E.”

Comment 17

Page 8, line 6, after Chimonas, 1970; add a reference <https://doi.org/10.1002/2016GL069740> as these authors directly reported related results based on GNSS TEC observations and other measurements. Very recently, Jonah et al., (2018), available on <https://doi.org/10.1029/2018JA025367>, reported related results during storm conditions. Consult this reference as well (I think their Figure 4). On this point, <https://doi.org/10.1002/2017JA024510>

Section 1. Reply to the Review Comments #1

1 reported equatorward LSTID propagating from the southern hemisphere crossing to the northern
2 hemisphere in the Asian region during this storm period. In fact, their analysis showed that these
3 TIDs may not have exceeded 30 degrees North, which may be in agreement with your analyses
4 and is more clearer in Figure 8(c) at around 1200 UT. Please have a look at their Figure 3(e) and
5 possibly add some discussion to this effect.

6 **Reply 17**

7 Thank you for the recommended references. They are added in the text and the logical
8 structure of the text is changed accordingly.

9 **The sentence in the original manuscript**

10 “Besides, the perturbations at 20°N around 12:00 UT and 13:00 UT show patterns of
11 poleward movement. Ding et al. [2013] have studied the poleward-propagating LSTIDs in
12 southern China during a medium-scale storm in 2011. They attribute their observations to the
13 excitation of secondary LSTIDs during the dissipation of primary disturbances from the lower
14 atmosphere. In addition, the poleward-moving disturbances may also be induced by the variation
15 of the equatorial electrojet [Chimonas, 1970] or just propagate from the southern hemisphere
16 [Zakharenkova et al., 2016]. A detailed investigation of this phenomenon is not the focus of this
17 work.”

18 **is revised as:**

19 **Page 9, Lines 6-18:** “Besides, the perturbations at 20°N around 12:00 UT and 13:00 UT
20 show patterns of poleward movement. Habarulema et al. [2018] have identified TIDs in the
21 Asian-Australian sector during the same storm period. It provides clear examples of TIDs crossing
22 the dip equator from the southern hemisphere to the northern hemisphere around 09:00-12:00 UT.
23 Their analysis shows that these TIDs may not have exceeded 30°N. Such poleward feature is also
24 detected in other longitudinal sectors during this storm [Zakharenkova et al., 2016] and other
25 storms [Pradipta et al., 2016; Jonah et al., 2018]. In addition, Ding et al. [2013] have studied the
26 poleward-propagating LSTIDs in southern China during a medium-scale storm in 2011. They
27 attribute their observations to the excitation of secondary LSTIDs during the dissipation of
28 primary disturbances from the lower atmosphere. Besides, the poleward-moving disturbances may
29 also be induced by the variation of the equatorial electrojet as pointed out by Chimonas [1970] and
30 more recently by Habarulema et al. [2016]. A detailed investigation of this phenomenon is not the
31 focus of this work.”

32 **New added References**

33 **Page 14, Lines 39-42:** Jonah, O. F., Coster, A., Zhang, S., Goncharenko, L., Erickson, P. J., Paula,
34 E. R., and Kherani, E. A.: TID observations and source analysis during the 2017 Memorial
35 Day weekend geomagnetic storm over North America. *Journal of Geophysical Research:*
36 *Space Physics*, 123, 8749– 8765. <https://doi.org/10.1029/2018JA025367>, 2018.
37

38
39
40 **Accordingly, some statements in the Discussion section are rephrased since new references**
41 **are included. For example:**

42
43 “Zakharenkova et al. [2016] have studied the behaviors of LSTIDs during the St. Patrick’s
44 Day storm for the European and American sectors with GPS and GLONASS observations. It

Section 1. Reply to the Review Comments #1

1 shows clearly in their results that the European sector (10°E) also exhibits LSTIDs around 11:00
2 UT. ... The fitting lines are obtained with a similar method mentioned above.

3 Figure 10 is basically consistent with the Figure 3(b) in Zakharenkova et al. [2016], such
4 as ...”

5 **is revised as:**

6 **Page 10, Lines 38-41 ~ Page 11, Lines 5-7:** “During the 2015 St. Patrick’s Day storm,
7 LSTIDs in the European-African, American and Asian-Australian sectors are detected and
8 analysed with TEC observations [Borries et al., 2016; Zakharenkova et al., 2016; Habarulema et
9 al., 2018]. It shows clearly in their results that the European sector also exhibits LSTIDs around
10 11:00 UT. The fitting lines are obtained with the same method as those in Figure 8.

11 Figure 10 is basically consistent with previous results, such as”

13 Summary:

15 **Comment 18**

16 Page 10, lines 1-3: The authors may want to rephrase this statement given that an earlier
17 study by Habarulema et al., (2018)– <https://doi.org/10.1002/2017JA024510> - provided some
18 analysis for this particular storm in the Asian sector. May be the analyses was not as detailed as
19 provided in this paper, but definitely this is not the first analysis for this storm in the Asian region.
20 The strength of this paper over what was presented in Habarulema et al., (2018) and other
21 attempted studies is the use of multiplicity of data sources to provide more details and clarity
22 during this storm period.

23 **Reply 18**

24 Thanks for pointing out this inappropriate statement. We have revised our text accordingly.

25 “Using data from 4 GPS receiver networks (CMGN, CMONOC, GEONET, IGS), together
26 with recordings of 2 HF Doppler shift stations and 8 ionosondes, we show the first observation
27 results of the LSTIDs in the East Asian sector during the 2015 St. Patrick’s Day storm.”

28 **is revised as:**

29 **Page 11, Lines 25-28:** “Using data from 4 GPS receiver networks (CMGN, CMONOC,
30 GEONET, IGS), together with recordings of 2 HF Doppler shift stations and 8 ionosondes, we
31 provide comprehensive and detailed observation results of the LSTIDs in the East Asian sector
32 during the 2015 St. Patrick’s Day storm.”

Reply to the Review Comments #2

The manuscript addresses the interesting scientific problem of understanding the properties of large scale travelling ionospheric disturbances (LSTIDs), which are frequently observed during geomagnetic storms. This manuscript discusses the properties of LSTIDs during 17th March 2015 with focus on the Chinese and Japanese sector. Although, descriptions of LSTID occurrence during this event have been published before, this manuscript adds new aspects on the longitudinal dependence of the LSTID properties in the Chinese/ Japanese sector based on GNSS, HF and ionosonde data. The manuscript is well structured, well written and presents analysis of high quality in a well understandable way. Thus, my overall evaluation is publishing after solving minor remarks. The manuscript in its current form has three weak points.

Thank you for your substantial and detailed comments here and in the supplement material! According to these comments, we revised the manuscripts and gave our replies to these comments point by point. The original manuscript, the revised version and the added references are listed if necessary. The red colors mark the revised parts and the new references.

Note that this reply is focusing on the Review Comments #2. The revised parts and the new references according to the Review Comments #1 are marked with yellow highlights when there are overlaps.

Reply to Major Comment:

Major Comment I.

I. First, already in the abstract the authors are referring to negative and positive LSTIDs and seem to treat them in the course of the manuscript like separate phenomenon. Since these LSTIDs are the signature of atmospheric gravity waves, both signatures belong to the same wave. Therefore, I would recommend to avoid discussing positive and negative amplitudes separately.

Related Annotation: measuring wave trough and crest should be rather the same, since they belong to one phenomenon, which is the gravity wave. However, the wave properties might change with time dependent on the forcing. This might explain the differences of both measurements. Looking at the error margins, both V_t and V_c indeed overlap (although only marginally). This is good.

Reply I.

Thank you very much for these suggestions!

Firstly, we misused phrases of “negative and positive LSTIDs”. They should be “the trough and crest of the LSTID”. This has also been pointed out by the Review Comments #1. We have revised those misleading statements accordingly. Besides, because the scale of this LSTID (period and wavelength) is very large and cover large spatial region, the wavefront of the LSTID maybe deformed due to different background condition during its propagation from higher to lower latitude, we discussed the trough and crest of the LSTID separately since they behave differently,

Section 2. Reply to the Review Comments #2

1 which can be seen in our results. This may be attributed to, as the reviewer suggest, that the wave
2 properties change with time dependent on the forcing. Meanwhile, V_t and V_c show certain
3 consistency. We have revised our manuscript accordingly to make these clear. To be specific:

4 **The statement**

5 “Besides, it is interesting to note that the mean V_c is slightly larger than the mean V_t , which
6 seems like the wave behind is pushing that ahead.”

7 **is revised to**

8 **Page 8, Lines 28-33:** “ V_t and V_c overlap, although only marginally, considering the error
9 ranges. Meanwhile, the mean V_c is slightly larger than the mean V_t , which seems like the wave
10 behind is pushing that ahead. In general, the speed of trough and crest of the LSTID should be
11 rather the same since they are induced by the same gravity wave. However, the wave properties
12 might change with time dependent on the forcing from background condition, especially for
13 LSTID covering large spatial region. This might explain the differences.”

14 **Major Comment II.**

15 **II. Second, the key point of the manuscript is the discussion of longitudinal dependence of**
16 **LSTID properties. But, this is impacted by the data coverage. The data coverage is**
17 **lower in the east and west boundaries of the investigated region. I argue that this**
18 **impacts the accuracy of the estimation of the LSTID properties. The discussion of the**
19 **LSTID properties (wavelength, period and speed) should be treated with more care**
20 **concerning reliability of the results.**

21 **Related Annotation.** Please elaborate on the impact of data coverage and size of the regions
22 of investigation on the accuracy of the results. The regions used for the Time-Latitude
23 Plots cover about 20° in latitude. This is roughly one wavelength. If the data coverage is
24 reduced (what is the case in the East and West regions), this introduces certainly an
25 error on the results.

26 **Related Annotation.** Nice figure and good illustration. Again, I am requesting to elaborate on
27 the accuracy of the results. The deviation between geomagnetic declination and wave
28 propagation direction is largest in the East and West, where you have lower data
29 coverage.

30 **Related Annotation.** I see it critical to highlight this fact, on the one hand because there is no
31 clear dependence and explanation for the longitudinal tendency and on the other hand,
32 it might be impacted by the measurement properties.

33 **Reply II.**

34 Thank you very much!

35 Indeed, the data coverage in the East and West boundaries of the studied region is relatively
36 lower comparing to that between 100°E - 120°E . Such difference in data coverage is resulted from
37 both GPS-receivers and land-sea distributions. Besides, the studied latitudinal range is $\sim 20^\circ$,
38 which is roughly one wavelength as the reviewer pointed out.

39 Meanwhile, it should be noted that we do had considered these issues in the manuscript and
40 tried our best to reduce such influences. For example, we selected areas for every 10 longitudinal
41 degrees with varying latitudinal ranges (Figure 7) to include as many data points as possible. Data
42 in longitudinal bands of 70°E - 80°E and 140°E - 150°E were not used considering the bad data
43
44

Section 2. Reply to the Review Comments #2

1 coverage. Besides, data in every 0.1-hours bin in TLPs (Figure 8) was obtained by latitudinal
2 average for every 10° longitudinal band. We find that data in 130°E-140°E is hugely influenced by
3 data coverage, so it has not been used when deriving LSTID parameters. In addition, since the
4 studied latitudinal range is roughly one wavelength, it is hard to estimate the wavelength directly
5 from the 2D VTECP map. Instead, the wavelength is estimate with the velocity and period from
6 TLPs.

7 Of course, these cannot totally eliminate the data-coverage influence to the estimation
8 accuracy of the LSTID parameters. Our results should be examined by further studies with better
9 data coverage in a wider longitudinal range.

10
11 **The statement**

12 “Finally, with the period and speed, the wavelength can be easily determined.”

13 **is revised to**

14 **Page 8, Lines 17-20:** “As for the estimation of wavelength, note that the studied area is ~ 20°
15 in latitude, which is roughly one wavelength and thus make it difficult to estimate the wavelength
16 directly from the 2D VTECP’ map. So, the wavelength is derived from the multiplication of speed
17 and period.”

18
19 **The statement**

20 “The longitudinal dependence of these parameters can be seen clearly.”

21 **is revised to**

22 **Page 8, Lines 23-26:** “It can be seen that these parameters show certain longitudinal
23 dependence. It should be noted that the data coverage is relatively lower in the east and west
24 boundaries of the investigated region. This may impact the accuracy of the estimation of the
25 LSTID properties in these areas.”

26
27 **The statement**

28 “It should be noted that our speculation needs to be verified with more observational data and
29 numerical simulation to reduce uncertainty in our propagation estimation and to figure out the
30 detailed physical processes.”

31 **is revised to**

32 **Page 10, Lines 34-37:** “Besides, considering the relatively low data coverage in the
33 East/West side of the studied region, it should be noted that our speculation needs to be verified
34 with more observational data and numerical simulation to reduce uncertainty in our propagation
35 estimation and to figure out the detailed physical processes.”

36
37 **The statement**

38 “(3) Other propagation parameters are also longitudinal dependent (see Table 1), and the
39 mean values and standard deviations of the period, V_t , V_c , and wavelength are 74.8 ± 1.4 minutes,
40 578 ± 16 m/s, 617 ± 23 m/s, and 2691 ± 80 km, respectively.”

41 **is revised to**

42 **Page 11, Lines 40-41 ~ Page 12, Lines 1-6:** “(3) The propagation parameters in different
43 longitudinal bands are estimated. These parameters show certain longitudinal dependence. Besides,
44 the mean values and standard deviations of the period, V_t , V_c , and wavelength are 74.8 ± 1.4

Section 2. Reply to the Review Comments #2

1 minutes, 578 ± 16 m/s, 617 ± 23 m/s, and 2691 ± 80 km, respectively.

2 It should be noted that our results show certain consistency with previous works focusing on the
3 Chinese or Japanese sector for different LSTID events. Nevertheless, the longitudinal dependence
4 shown in our results should be examined further with more case studies based on large
5 longitudinal and high-resolution coverage of GPS data.”

6 ”.

9 **Major Comment III.**

10 **III. Third, the authors present also the result of the LSTID occurrence in Europe. This has**
11 **been extensively discussed in Borries et al. (2016, <https://doi.org/10.1002/2016JA023178>).**
12 **Specifically, the LSTID occurring between 11 and 12 UT has been discussed to be**
13 **“special” because it is impacted by winds and prompt penetration electric fields at the**
14 **same time. This fact should be included in the discussion of this manuscript. It supports**
15 **the finding of the authors that the LSTID properties in Europe differ from the LSTID**
16 **properties in the Chinese/ Japanese sector.**

17 **Related Annotation: Borries et al. (2016) shows and discusses some more details about the**
18 **LSTIDs. The LSTID between 11 and 12 UT is specifically large and a combination of**
19 **wind and electric field effects.**

20 **Related Annotation: The reason for the difference are the different physical processes that**
21 **compete over Europe (as described in Borries et al., 2016).**

22 **Related Annotation: It is not clear why these LSTIDs can be only driven by winds. Please**
23 **elaborate what would be the difference in case these TEC perturbations would be**
24 **driven by electric fields.**

26 **Reply III.**

27 Thank you very much for recommending this reference!

28 Actually, after the manuscript submission, we noticed that we missed this reference. This
29 paper has also been recommended by the Review Comments #1. We have already added it into the
30 revision.

31 According to this comment and related annotation, the statements about the difference
32 between East-Asian and European sectors focusing on PPEF are added accordingly.

35 **The statement**

36 “In addition, the tendency of field-aligned propagation of the LSTID indicates that it is
37 driven by the neutral winds rather than by electric fields since the winds push the plasma up and
38 down along the magnetic field lines.”

39 **is revised to**

40 **Page 10, Lines 29-34: “In addition, the tendency of field-aligned propagation of the LSTID**
41 **indicates that it is driven by the neutral winds since the winds push the plasma up and down along**
42 **the magnetic field lines. There is no evidence, such as simultaneous perturbations at all latitudes in**
43 **other cases [Borries et al., 2016; Zakharenkova et al., 2016], to show that the LSTID in the**
44 **Chinese/Japanese sector is affected by prompt penetration electric field (PPEF) during the same**

Section 2. Reply to the Review Comments #2

1 period.”

2 **Statements below are added.**

3 **Page 11, Lines 15-19:** “Borries et al. [2016] present a detailed study on the LSTID in Europe
4 during this storm. It is suggested that the perturbation occurring around 11:00 UT is special since
5 it is impacted by PPEF and wind at the same time. Comparatively, the LSTID in the
6 Chinese/Japanese sector seems only driven by winds. This may partly account for the longitudinal
7 difference in our results.”

11 **Technical Recommendations/Corrections:**

12 **Comment 1**

13 **Jakowski et al. (2008) did not discuss LSTIDs but large scale gradients (no discussion of**
14 **wave properties)**

15 **Reply 1**

16 Thank you very much! **This reference has been deleted** in the revised article.

17 **Comment 2**

18 **URLs of the data sources are usually provided in the acknowledgements, not in the text.**

19 **Reply 2**

20 Thank you very much! URLs of the data sources have been **moved into the acknowledgements.**

21 **Comment 3**

22 **Presenting the LSTID results with VTECP' has the advantage of better illustrating most**
23 **wave properties, but it does not represent the true wave amplitude anymore. On a quick**
24 **view, the figures might be misinterpreted. Therefore, I recommend to make it very clear**
25 **that this is an “artificial” amplitude.**

26 **Related Annotation: This is certainly nice to better visualize the positive and negative**
27 **amplitude of the TEC perturbation. But the authors should take care, that the readers**
28 **do not misinterpret the amplitude of the TEC perturbation. It looks like the Amplitude**
29 **is about 2 TECU, but is that the true amplitude?**

30 **Reply 3**

31 Thank you very much for this suggestion! We have revised the manuscript accordingly.

32 **The statement**

33 “Note that the raw value of VTECP is converted into VTECP' with

$$34 \quad VTECP' = \text{sgn}(VTECP) * \log_{10}(\text{abs}(VTECP) + 1)$$

35 to make it easier to distinguish the regions with positive and negative perturbations.”

36 **has been revised to:**

37 **Page 6, Lines 2-8: “The raw value of VTECP has already been converted into VTECP' with**
38 **the equation**

$$39 \quad VTECP' = \text{sgn}(VTECP) * \log_{10}(\text{abs}(VTECP) + 1)$$

40 **(3)**

Section 2. Reply to the Review Comments #2

1 The raw amplitude of VTECP above 30°N is ~ 2 TECu while the raw amplitude of VTECP below
2 30°N reaches ~ 10 TECu. So, transform (3) provides a better colormap for 2D VTECP plots by
3 sharpening the edges between positive and negative values and reduce the differences of VTECP
4 in middle and low latitudes. Consequently, it should be noted that the amplitude of the wavelike
5 variation does not represent the true wave amplitude but an “artificial” one.”

The Figure 4 caption

6
7
8 “Figure 4. A series of 2D VTECP’ maps over the East Asian sector from the period of
9 09:40-09:50 UT to 11:30-11:40 UT on 17 March 2015. The grey areas represent the nightside. The
10 colorbar represents the VTECP’ (units: TECu). The lime and yellow lines illustrate the least square
11 fittings (order 2) for wavefronts.”

is revised as

12
13 **Page 17, Lines 13-17:** “Figure 4. A series of 2D VTECP’ maps over the East Asian sector
14 from the period of 09:40-09:50 UT to 11:30-11:40 UT on 17 March 2015. The grey areas
15 represent the nightside. The colorbar represents the VTECP’ (units: TECu), which is transformed
16 from the original VTECP value with equation (3) for a more viewer-friendly colormap. The green
17 and yellow lines illustrate the least square fittings (order 2) for wavefronts.”

Comment 4

18
19
20 **Figures 3 and 5 do not have much content. But they are supposed to be compared with each
21 other. Therefore, I recommend to join the content of both figures into one figure. This
22 will increase the information density and allow better comparability.**

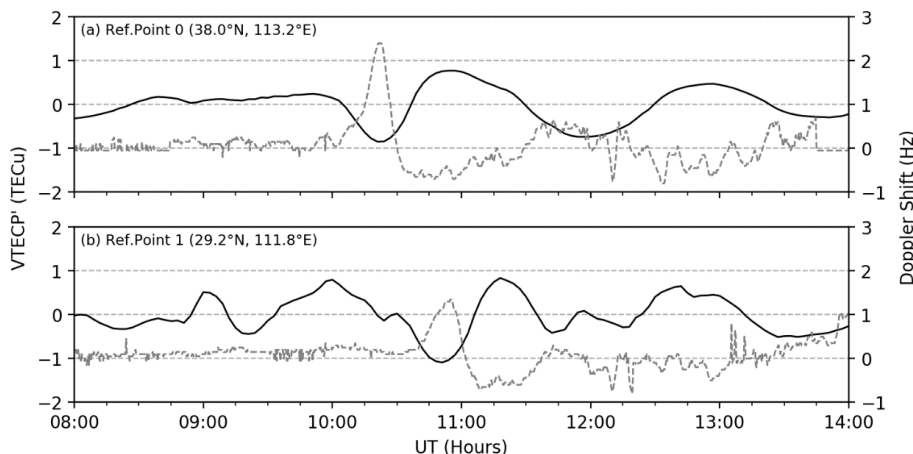
23 **Related Annotation:** I think, it would be nice to join Fig3 and Fig 5 to one plot, to have a
24 more direct comparison of peaks in both plots and better visualize the similarities.

Reply 4

25 Thank you very much!

26 It is a good idea to combine Figure 3 and 5 together to have a more direct comparison.
27 However, combining them together will change the logical frame of the manuscript and a lot of
28 places need to be rewritten considering the context. So, we plot the variation of doppler shifts into
29 Figure 5.

Figure 5 is revised to



30
31
32
33 **Figure 5 description is expanded to**

Section 2. Reply to the Review Comments #2

1 **Page 17, Lines 18-20:** “Figure 5. Temporal variations of mean VTECP’ near the Doppler
2 reflection points between 08:00 UT and 14:00 UT, 17 March 2015. Doppler shift recordings in
3 Figure 3 are plotted with dashed lines for comparison.”

4
5 **The statement below is added.**

6 **Page 6, lines 38-39:** “Doppler shift recordings in Figure 3 are also plotted with dashed lines
7 for comparison.”

9 **Comment 5**

10 **In figure 8, the impact of EIA is addressed. I assume, the dashed black lines indicate the**
11 **boundary of EIA. This should be made clear in the text and figure description**

12 **Related Annotation:** Please include a sentence describing, how the reader is going to identify
13 the EIA region. I assume, the black dashed lines are encapsulating this region.

14 **Reply 5**

15 Thank you very much! The manuscript has been revised accordingly.

16 **The statements**

17 “As mentioned before, the variation of VTECP’ in the EIA region is rather complex, so only
18 the values over 30°N (marked with dashed lines) are used to estimate the speed.”

19 **is revised to**

20 **Page 8, Lines 2-5:** “As mentioned before, the VTECP’ variation related to EIA is rather
21 complex. Considering that EIA is mainly a low-latitudinal phenomenon, the 30°N is marked with
22 black dashed lines in Figure 8 which indicate the boundary of EIA. Only values over 30°N are
23 used to estimate the speed.”

24 **Figure 8 caption**

25 “Figure 8. TLPs of VTECP’ for different longitudinal bands between 07:00-14:00 UT. White
26 dots give the data points for linear fitting, and the fitting results are marked with white lines. Black
27 dashed lines depict 30°N in (b-d, f) and 40°N in (f).”

28 **is revised as**

29 **Page 17, Lines 28-31:** “Figure 8. TLPs of VTECP’ for different longitudinal bands between
30 07:00-14:00 UT. White dots give the data points for linear fitting, and the fitting results are
31 marked with white lines. 30°N in (b-d, f) is marked with black dashed lines which indicate the
32 boundary of EIA. 40°N is marked in (f).”

34 **Comment 6**

35 **In the discussion section, the authors exclude the impact of electric fields on the LSTID**
36 **propagation and favour the impact of winds, driving the LSTID propagation because of**
37 **field-aligned propagation. For a better understanding, the authors should explain, what**
38 **would be different in case of electric field impact. In fact, since Borries et al. (2016)**
39 **describe prompt penetration electric field impact in Europe at that time, more emphasis**
40 **should be given to discuss electric field impact in the Chinese/Japanese sector at the**
41 **same time.**

42 **Reply 6**

43 Thank you very much for this suggestion! This Comment is related to the **Major Comment III**.
44 Please refer to replies to in that section in page 2.

Section 2. Reply to the Review Comments #2

1

2

Comment 7

3

I detected a few spelling errors and grammar issues (indicated in the supplementary material). I expect, there are more than I found and recommend professional editing.

4

5

Reply 7

6

Thank you very much!

7

We have revised all the spelling errors and grammar issues that indicated in the supplementary material. We have further checked throughout the article and found several other errors and they have also been revised in the revision. All of them are marked with red color in the supplement material.

8

9

10

11

1 **A case study of the large-scale traveling ionospheric disturbances in the East Asian sector**
2 **during the 2015 St. Patrick's Day geomagnetic storm**

3 Jing Liu¹, Dong-He Zhang^{1*}, Anthea J. Coster², Shun-Rong Zhang², Guan-Yi Ma³, Yong-Qiang
4 Hao¹, Zuo Xiao¹.

5 1, Department of Geophysics, Peking University, Beijing, China, 100871

6 2, MIT Haystack Observatory, Westford, Massachusetts, USA

7 3, National Astronomical Observatories, Chinese Academy of Sciences, Beijing, China

8

9 **Abstract**

10 This study presents a comprehensive observation of the large-scale traveling ionospheric
11 disturbances (LSTIDs) in the East Asian sector during the 2015 St. Patrick's Day (March 17, 2015)
12 geomagnetic storm. For the first time, 3 dense networks of GPS receivers in China and Japan are
13 combined together to obtain the 2-dimensional (2D) vertical total electron content (VTEC)
14 perturbation maps in a wider longitudinal range than previous works in this region. Results show
15 that a trough of LSTID spanning at least 60° in longitude (80°E-140°E) occurs and propagates
16 from high to lower latitudes around 09:40-11:20 UT. It is followed by a crest of LSTID which
17 shows a tendency of dissipation starting from the East side. The manifestation of the 2D VTEC
18 perturbation maps is in good agreement with the recordings from 2 high-frequency Doppler shift
19 stations and the iso-frequency lines from 8 ionosondes. Then, the propagation parameters of the
20 LSTIDs are estimated by applying least square fitting methods to the distinct structures in the 2D
21 VTEC perturbation plots. In general, the propagation parameters are observably longitudinal
22 dependent. For example, the propagation direction is almost due southward between 105°E-115°E,
23 while it is slightly South by West/East in the West/East side of this region. This feature is probably
24 related to the regional geomagnetic declination. The mean values of the period, trough velocity
25 (V_t), crest velocity (V_c), and wavelength of the wavelike LSTIDs in the studied longitudinal
26 bands are 74.8 ± 1.4 minutes, 578 ± 16 m/s, 617 ± 23 m/s, and 2691 ± 80 km, respectively. Finally,
27 using the VTEC map data from the Madrigal database of the MIT Haystack Observatory, the
28 characteristics of the ionospheric disturbances over the European sector (30°N-70°N, 10°E-20°E)
29 are also studied. The results are very different from those in the East Asian sector in parameters
30 like the occurrence time, oscillation period, and propagation velocities.

31 **Keywords: Geomagnetic Storm; LSTID; GPS TEC.**

32

33

34

1 **1. Introduction**

2 During the geomagnetic storm, the solar wind energy is impulsively or continually injected into
3 the earth polar region and making the atmospheric and ionospheric states deviate greatly from
4 their background levels [Fuller-Rowell et al., 1994]. In general, the response of the ionosphere to
5 the geomagnetic storm is classified by a variety of different features, one of which is the large
6 scale traveling ionospheric disturbance (LSTID) that is the wave-like perturbation mainly
7 propagating equatorward from high latitudes. Traveling ionospheric disturbances (TIDs) are
8 classified into LSTIDs and Medium-scale TIDs and they are considered to be the ionospheric
9 manifestation of the presence of atmospheric gravity waves (AGWs) stimulated by different
10 sources. LSTIDs are mainly caused by Joule heating or Lorenz-drag forcing in the Auroral regions
11 during geomagnetic storm period [Hines, 1960; Richmond and Roble, 1979; Hocke and Schlegel,
12 1996].

13 In earlier years, the acquisition of the continuous evolution of LSTIDs on a global scale was
14 limited by the availability of the ionospheric observations. In order to obtain the propagation
15 characteristics of LSTIDs on a large spatial scale, researchers needed to organize their findings
16 from limited ionospheric observations, for example, the foF2 data from sparsely distributed
17 ionosondes. In the 1980s, the **GPS (Global Positioning System)** method was introduced into the
18 ionospheric study [Klobuchar, 1986; Lanyi and Roth, 1988; Coster and Gaposchkin, 1989]. With
19 the dense and worldwide distributed GPS receivers, some characteristic ionospheric phenomena,
20 like traveling ionospheric disturbances (TIDs) [Saito et al., 1998; Tsugawa et al., 2004; Ding et al.,
21 2007], ionospheric storms [Ho et al., 1996], and ionospheric responses to solar flares
22 [Afraimovich, 2000a; Zhang and Xiao, 2005] were revisited frequently and new results were
23 obtained.

24 The propagation characteristics of LSTIDs are always topics of great research interest [Hunsucker,
25 1982; Ho et al., 1996; Balthazor and Moffett, 1999; Afraimovich et al., 1998, 2000; Shiokawa et
26 al., 2002; Tsugawa et al., 2003, 2004; Ding et al., 2008, 2014; Borries et al., 2009, 2017;
27 Habarulema et al., 2015, 2016, 2018; Zakharenkova et al., 2016; Figueiredo et al., 2017; Pederick
28 et al., 2017; Cherniak et al., 2018; Lyons et al., 2019]. Based on limited GPS stations
29 measurements, Afraimovich et al. [1998] propose a radio interferometry method to roughly
30 estimate horizontal propagation velocities and phase front angles of TIDs. Further, the world-wide
31 or local dense distribution of the GPS receivers networks facilitates the acquisition of the global or
32 regional TEC perturbation maps with high spatial and temporal resolutions to reveal the detailed
33 propagating characteristics of TIDs [Ho et al., 1996; Saito et al., 1998; Tsugawa et al., 2004;
34 Borries et al., 2009; Ding et al., 2012]. With more than 60 GPS receivers distributed worldwide,
35 Ho et al. [1996] studied the global distribution of TEC variations and perturbations during a
36 magnetically disturbed period. They identified a TID propagating from the northern sub-auroral
37 region to lower latitudes at a speed of about 460 m/s. The GPS Earth Observation Network
38 (GEONET) in Japan is one of the densest GPS receiver networks on the Earth, and utilizing its
39 data **two-dimensional** (2D) TEC perturbations over Japan can be mapped. With these
40 high-resolution TEC perturbation maps, the spatial structures and temporal evolutions of a TID in
41 the nighttime mid-latitude ionosphere over Japan were revealed clearly [Saito et al., 1998]. Since
42 then, with this dense GPS network, the characteristics of LSTIDs over Japan are carefully studied
43 through case and statistical analysis, and some propagation features of TIDs in this region are

1 revealed [Saito et al., 2001; Shiokawa et al., 2002; Tsugawa et al., 2003, 2004, 2006].

2 For the LSTID with scales of thousands of kilometers, the extensive spatial coverage of
3 ionospheric observations is undoubtedly useful for capturing its propagation features. In recent
4 years, the GPS data from densely distributed GPS stations in China are used to study LSTIDs in
5 this region [Ding et al., 2012, 2013, 2014; Song et al., 2013]. Based on the GPS data from the
6 Crustal Movement Observation Network of China (CMONOC), Ding et al. [2012] obtains
7 temporal continuous 2D imaging of ionospheric disturbances during the geomagnetic storm on
8 May 28, 2011, and find two LSTIDs moving southwestward with the front width of at least 1600
9 km during different storm phases. In addition, through the comparative climatological study of
10 LSTID over North America and China, the different time dependence of LSTID occurrence over
11 two longitudinal sectors were revealed statistically [Ding et al., 2014]. These studies further
12 emphasize the effectiveness of the large coverage, high-resolution ionospheric observations from
13 GPS networks on the detailed investigation of structures of the ionospheric disturbances.

14 The propagating direction of the LSTID during the geomagnetic storm has always been focused
15 on for the LSTID studies. From case and statistical studies about LSTID during geomagnetic
16 storm period over East-Asia region conducted independently by Chinese and Japanese scientists in
17 recent years, the dominant propagating direction of LSTID in China and Japan is a little different.
18 It mainly propagates South by West in the Chinese region [Ding et al., 2014], while it mainly
19 propagates South by East in the Japanese region [Tsugawa et al., 2004]. Although the geomagnetic
20 declination is considered to be one of the main factors to be responsible for the propagation
21 direction of LSTID based on different LSTID studies, the LSTID studies concerning the same
22 geomagnetic storm using both Chinese and Japanese GPS networks together have not yet been
23 reported.

24 During the period of 17–18, March 2015, the strongest geomagnetic storm in the 24th solar cycle
25 occurred and LSTIDs are detected and analysed in different longitudinal sectors [Ramsingh et al.,
26 2015; Borries et al., 2016; Zakharenkova et al., 2016; Habarulema et al, 2018]. Meanwhile, two
27 high frequency (HF) Doppler stations operated by China Meridional Project [Wang, 2010] at
28 mid-latitude China record large ionospheric HF Doppler shifts after 10:00 UT, which seem to
29 indicate the LSTIDs in the Asian region between 09:00-12:00 UT that reported by Habarulema et
30 al. [2018]. In this study, the multi-network of densely distributed GPS receivers, the HF Doppler
31 stations, and an ionosonde network are used to conduct a more comprehensive study on the
32 propagating characteristics of the disturbances in the East Asian region, especially on the
33 characteristics of the dominant propagating direction over China and Japan.

34 **2. Data and Methods**

35 Figure 1 illustrates the locations of ground-based receivers that are used in this study from 4
36 Global Navigation Satellite Systems (GNSS) networks distinguished by colors. They are Chinese
37 Meteorological GNSS Network (CMGN), CMONOC in China, GEONET in Japan, and
38 International GNSS Service (IGS). These receivers are selected through data quality checking and
39 regional restriction ($10^{\circ}\text{N} \sim 60^{\circ}\text{N}$, $70^{\circ}\text{E} \sim 150^{\circ}\text{E}$), and the numbers of used stations are 259, 220,
40 1300, and 31 for CMGN, CMONOC, GEONET, and IGS, respectively. The sample rate of all GPS
41 data is 30 seconds. Combining the carrier phase and pseudo-range measurements in two L-band
42 frequencies of GPS receivers' observations, the vertical TEC can be obtained. In the calculation,

Section 3. Marked-up Manuscript

1 the height of the ionospheric thin shell is set to be 400 km, and the cutoff elevation angle is 30
2 degrees. The detailed process of the TEC calculation from GPS data can be found in our previous
3 works [Zhang et al., 2009; Zhang et al., 2010].

4 Different methods have been used for extracting the TEC perturbations related to LSTIDs in
5 previous works [Wan et al., 1997; Afraimovich et al., 2000; Shiokawa et al., 2002; Nicolls et al.,
6 2004; Tsugawa et al., 2004; Ding et al., 2007]. Afraimovich et al. [2000] suggest that the LSTID
7 characteristics in TEC can be determined by removing the trend with 3 to 5 order polynomials in
8 order to eliminate the trends introduced by the motion of satellites and variations of the regular
9 ionosphere. For a similar purpose, Shiokawa et al. [2002] subtract a running average of TEC over
10 1 hour from the raw TEC. With more than 1000 GPS receivers over Japan, a series of 2D TEC
11 perturbation maps can be obtained. Ding et al. [2007] develop another method of obtaining the 2D
12 TEC perturbation maps by expressing the vertical TEC as a one-order function of local time and
13 latitude. According to their argument, this method is sufficient to remove background trends for
14 continuous observation of a GPS receiver-satellite pair without introducing artificial perturbations.
15 After comparing the results of these methods, a method similar to Ding et al. [2007] is conducted
16 in this study, in which the vertical TEC at an ionospheric pierce point (IPP) is treated as a function
17 of universal time (UT), longitude (Lon), and latitude (Lat), i.e.,

$$VTEC_0 = C_0 + C_1UT + C_2Lon + C_3Lat \quad (1)$$

$$VTECP = VTEC - VTEC_0 \quad (2)$$

18 in which $VTEC_0$ is the background change and $VTECP$ is VTEC perturbation. Then, the obtained
19 $VTECP$ data is reorganized into pixels which are bounded by $10^\circ\text{N} \sim 60^\circ\text{N}$, $70^\circ\text{E} \sim 150^\circ\text{E}$ and
20 with a spatiotemporal resolution of 1° longitude \times 1° latitude \times 10 minutes. The $VTECP$ value for
21 each pixel is set to be the average of all $VTECP$ data of which the IPP and UT locate in this pixel.
22 After these steps, the featured ionospheric disturbances are expected to appear on a series of 2D
23 $VTECP$ maps.

24 As a comparison, the VTEC map from Madrigal database of the MIT Haystack Observatory is
25 used to reveal the ionospheric disturbances in the European sector ($30^\circ\text{N} \sim 70^\circ\text{N}$, $10^\circ\text{E} \sim 20^\circ\text{E}$).
26 This database provides worldwide VTEC values in 1° latitude \times 1° longitude pixels with a
27 temporal resolution of 5 minutes [Rideout and Coster, 2006] and has good data coverage in
28 European and American sectors. VTEC maps with such a high spatiotemporal resolution are
29 suitable to reveal the structures of traveling ionospheric disturbances [Zhang et al., 2017].

30 The Doppler shift data observed at two high frequency (HF) Doppler sounding stations in China is
31 collected, of which the station codes are MDT (40.4°N , 116.9°E), and SZT (22.6°N , 114.1°E). The
32 sounding system continuously receives electromagnetic waves with a stabilized frequency of 10
33 MHz transmitted by the National Time Service Center (NTSC) (35.7°N , 109.6°E) to detect the
34 ionospheric disturbances through the Doppler shifts of this standard frequency. These shifts are
35 considered to be caused by ionospheric variations mainly around the reflecting point of the
36 electromagnetic wave in the ionosphere. According to the geometrical relationships, the locations
37 of the reflecting point for MDT and SZT are (38.0°N , 113.2°E) and (29.2°N , 111.8°E), respectively.
38 These stations are marked in Figure 1 with colored stars.

39 In this study, ionograms from 8 ionosonde stations in China middle latitude are used to derive the

1 iso-frequency lines, which vary as a function of universal time and virtual height. The sample rate
2 of the ionograms is 15 minutes. These ionosondes belong to the China Research Institute of
3 Radio-wave Propagation (CRIRP) and their locations are marked in Figure 1 with green triangles.
4 The virtual height data is manually scaled by ourselves to reduce possible errors of auto scaling
5 [Krankowski et al., 2011; Habarulema and Carelse, 2016] from these ionograms with professional
6 scaling software provided by CRIRP. During the scaling, we limited the frequency to be less than
7 7 MHz. In addition, the condition of the geomagnetic storm is shown with data from the high
8 resolution (5 minutes) OMNI dataset, which is downloaded from the FTP service of the NASA
9 Goddard Space Flight Center.

10 3. Results

11 3.1 Observations

12 Figure 2 shows the variations of (a) solar wind speed, (b) interplanetary magnetic field (IMF) B_z
13 component, (c) the SYM-H index, and (d) the AE index from the OMNI dataset, and the time
14 range is from 18:00 UT, 16 March 2015 to 06:00 UT, 18 March 2015. It should be noted that the
15 solar wind magnetic field and plasma data are time-shifted to the bow shock nose to better support
16 the solar wind-magnetosphere coupling studies. It can be seen clearly that a geomagnetic storm
17 occurred on 17 March 2015, with the sudden storm commencement (SSC) at $\sim 04:45$ UT, which is
18 characterized by a sharp increase (marked with vertical dashed lines) in the solar wind speed, B_z ,
19 and SYM-H index. The main phase of the storm can be roughly divided into two stages. The first
20 stage is from $\sim 06:00$ UT, when the IMF B_z component first turns to southward, to $\sim 12:00$ UT,
21 when the B_z turns southward again after back to northward for about 2 hours. After $\sim 12:00$ UT,
22 the B_z is southward for most of the time, until it enters the recovery phase. The SYM-H and AE
23 indices show a similar two-stage feature as the B_z . SYM-H decreases after $\sim 06:00$ UT, reaches
24 the first minimum at $\sim 09:30$ UT, and increases to a local maximum at $\sim 12:00$ UT. Then, it
25 gradually decreases with small oscillations and reaches the minimum value of -233 nT at $\sim 22:45$
26 UT. Correspondingly, the AE index exhibits the first increase period between 06:00 UT to 12:00
27 UT, with the maximum intensity of ~ 1000 nT, and the second period between 12:00 UT to 02:00
28 UT of the next day, during which the AE increases much larger with several peaks. This storm is
29 the strongest one in the 24th solar cycle [Astafyeva et al., 2015].

30 During the first stage of the main phase, disturbances are observed successively at MDT and SZT
31 Doppler receiver stations. Figure 3 illustrates the variations of the Doppler shift records at (a)
32 MDT and (b) SZT between 08:00 UT and 14:00 UT on 17 March 2015. It shows that two distinct
33 positive shifts occur at about 10:22 UT and 10:53 UT, respectively. Shortly after, it exhibits two
34 negative shifts but with much smaller amplitudes. Suppose these successive disturbances indicate
35 a propagating perturbation, according to the estimated locations of the reflecting points that
36 mention above and the occurrence time of the two positive peaks, the approximate speed of this
37 perturbation is about 535 m/s. This value is much larger than the speed of the movement of the
38 ionospheric negative storm that usually occurs in the middle latitude due to storm-induced
39 equatorward wind [Buonsanto, 1999], and the ionospheric storm is not serious in the Asian sector
40 during this period [Astafyeva et al., 2015]. Considering the magnitude of the speed and the time
41 interval of the positive-negative variations, the recorded perturbations probably reflect an
42 equatorward propagating LSTID in the East Asian sector.

Section 3. Marked-up Manuscript

1 To confirm this, Figure 4 presents a sequence of 2D VTECP maps between 09:40-11:40 UT on 17
2 March 2015 with the method described in section 2. The grey areas represent the nightside. The
3 raw value of VTECP has already been converted into VTECP' with the equation

$$\text{VTECP}' = \text{sgn}(\text{VTECP}) * \log_{10}(\text{abs}(\text{VTECP}) + 1) \quad (3)$$

4 The raw amplitude of VTECP above 30°N is ~ 2 TECu while the raw amplitude of VTECP below
5 30°N reaches ~ 10 TECu. So, transform (3) provides a better colormap for 2D VTECP plots by
6 sharpening the edges between positive and negative values and reduce the differences of VTECP
7 in middle and low latitudes. Consequently, it should be noted that the amplitude of the wavelike
8 variation does not represent the true wave amplitude but an “artificial” one. The yellow lines
9 illustrate the least square fitting results for all the negative pixels within certain rectangular areas
10 bounded by longitudes and latitudes. The green lines are similar but for pixels with the bottom 5%
11 absolute VTECP' values in selected areas (see section 3.2 for a detailed example). These two
12 kinds of lines mark the approximate locations of the wavefronts.

13 A large-scale wavelike perturbation can be seen clearly in Figure 4. The first relatively distinct
14 wave structure emerges during the (d) 10:10-10:20 UT period, while its sign can already be
15 observed as early as (a) 09:40-09:50 UT in the northwest part of China. During (e) 10:20-10:30
16 UT, a negative band occurs across both the Chinese and Japanese sectors between around
17 30°N-45°N, which gradually propagates to lower latitudes in the next tens of minutes. During (f)
18 10:30-10:40 UT, the first clear wavefront of the positive band appears, which also shows an
19 equatorward movement for at least half an hour. Finally, there seems to be no distinct wave
20 structure following the positive band. Considering the spatiotemporal characteristics of this
21 perturbation, it can be preliminarily identified as an LSTID. By the way, it is interesting to note
22 that the positive bands do not extend to the Japanese sector in (h) and (i), and the corresponding
23 VTECP' amplitudes seem smaller in the East side than in the West side. This may be related to the
24 fact that the Japanese sector has already entered the nightside.

25 Both the negative and positive bands exhibit more complex variations when they enter the
26 equatorial ionospheric anomaly (EIA) region between 20°N-30°N. On the one hand, the amplitude
27 of VTECP' is relatively larger than those in the higher latitudes. On the other hand, it seems that
28 the equatorward propagation of the negative band decelerates significantly in this area, which is
29 especially shown in (Figure 4, g-l). Such complex features are probably related to the various
30 physical processes in this region. Ding et al. [2012] suggest that LSTIDs experience severe
31 dissipation in South China region due to viscosity and heat conductivity at low latitudes, which
32 may account for the weakening of the equatorward propagating wavelike structures. Besides,
33 Pradipta et al. [2016] studied the interaction of the auroral LSTIDs from opposite hemispheres
34 near the dip equator during the 26 September 2011 geomagnetic storm. It shows that such
35 interaction may bring much complexity to the TEC perturbations near the dip equator.

36 Our observations of the Doppler shift and VTECP' maps are in good agreement. To show it
37 clearly, Figure 5 shows the variations of the mean VTECP' data near the Doppler reflection points
38 with the same time range of Figure 3. Doppler shift recordings in Figure 3 are also plotted with
39 dashed lines for comparison. It can be seen that the troughs at around 10:20 UT in (a) and 10:50
40 UT in (b) correspond well to the two distinct crests in Figure 3. In addition, the variations of the
41 VTECP' between 11:00 and 14:00 are also in a good negative correlation with the Doppler shift

1 observations for each reflecting point. It should be noted that the variation of VTECP' at the
2 reflecting point 1 exhibits more variability than that at the reflecting point 0, especially around
3 09:00 UT, 10:00 UT, and 12:00 UT. Considering that point 1 (29.2°N,111.8°E) is approaching the
4 EIA region, the causes for VTEC perturbations are more complicated as mentioned above. This
5 feature is consistent with the observations of the 2D VTECP' maps in Figure 4.

6 Ionospheric parameters from ionograms have been commonly used since early TID studies.
7 Recently, ionograms and iso-frequency lines with different sampling rates were used in TID
8 studies [Klausner et al, 2009; Ding et al., 2012, 2013; Pradipta et al., 2015; Ramsingh et al., 2015;
9 Habarulema et al., 2018]. Figure 6 presents the temporal variations of the virtual height for each
10 iso-frequency line. The names and locations of the corresponding ionosondes are given in each
11 subplot as annotates. The sampling frequency are marked on the right side for each line. On the
12 left column, the results of five stations are arranged in order from high to lower latitudes, and on
13 the right column, it shows the recordings of four stations in the same latitudinal belt. We can see
14 clearly that a distinct uplift of the virtual height occurs at 09:45 UT at Manzhouli station, and it
15 gradually moves equatorward from high to lower latitudes (Figure 6, a-e). Meanwhile, the phase
16 difference is not observed for the stations on the right column. This means that the ionospheric
17 disturbance roughly moves along the meridian line in this longitudinal sector (around 115°E),
18 which corresponds to the results of the 2D VTECP' map. Moreover, although the time resolution
19 of 15 minutes is relatively low, it can still be identified that the crests in the higher iso-frequency
20 lines appear earlier than those in the lower ones. Such trends (marked with black dashed lines)
21 indicate a downward vertical phase velocity, which is one of the typical characteristics of TID and
22 AGW [Hine, 1960; Hocke and Schlegel, 1996]. It should be noted that the downward trend is not
23 much clear for certain station, especially the one in Qingdao. This may be attributed to the 15
24 minutes sampling interval.

25 3.2 Estimating Propagation Parameters

26 As preparation for estimating the propagation parameters of this LSTID, Figure 7 shows a detailed
27 example of the wavefront fitting method with the VTECP' map in Figure 4(g) (10:40-10:50 UT).
28 The reason for choosing this period is that the structure of the wavefront is relatively clear, and the
29 boundary of the positive and negative wave band in the Japanese sector can still be partly
30 identified. The green line is the least square fitting for the green dots, of which the absolute
31 VTECP' values are close to zero (bottom 5%) among all the dots in a certain region (75°E-140°E,
32 30°N-40°N). The wave propagating azimuth (marked with arrows) can be estimated with the
33 normal direction of this fitting line. Results are listed in Table 1 in the second column.

34 It can be seen clearly that the TID moves due South around 110°E, and in the West/East region,
35 the propagation direction is slightly South by West/East. It should be noted that the morphology of
36 this TID is continuously changing as it moves from high to lower latitudes in the studied region.
37 Although the azimuths are estimated only with the wavefront data during 10:40-10:50 UT, such
38 longitudinal dependence of azimuths corresponds well with other fitting lines in Figure 4(e, f, g,
39 h).

40 In order to derive the phase speed, period, and wavelength of this LSTID, the time-latitude plots
41 (TLPs) of VTECP' are obtained for six longitudinal bands, which are marked with dashed
42 rectangles A-F in Figure 7. For each band, the VTECP' data is averaged along the latitude for

Section 3. Marked-up Manuscript

1 every 6 minutes (0.1 hours), and the results as a function of UT and latitude are illustrated
2 correspondingly in Figure 8 (a-f). As mentioned before, the VTECP' variation related to EIA is
3 rather complex. Considering that EIA is mainly a low-latitudinal phenomenon, the 30°N is marked
4 with dashed lines in Figure 8 which indicate the boundary of EIA. Only values over 30°N are used
5 to estimate the speed.

6 As expected, the most distinctive structures in all panels are the pair of negative and positive
7 bands around 10:40 UT, which correspond to the perturbations moving from high to lower
8 latitudes shown in Figure 4. The structures in the 130°E-140°E are not quite clear, which may be
9 due to the lack of data in some parts of this area, but the trough around 10:40 UT can still be
10 identified. To estimate the meridional phase speeds of these perturbation patterns, the linear least
11 square method is used to fit the pairs of troughs and crests. The data points for the linear fitting are
12 marked with white dots, which are the minimum/maximum values along with each latitudinal bin
13 around the negative/positive structures that we focus on. The phase speeds for wave troughs (V_t)
14 and crests (V_c) can be derived based on the slopes of the fitting lines. Moreover, the period of the
15 wave can be estimated through the time interval between the trough and crest in TLPs. In practice,
16 for each longitudinal region, the average of time lags along all latitudinal bins is set to be the half
17 period of the wave in this region. As for the estimation of wavelength, note that the studied area is
18 $\sim 20^\circ$ in latitude, which is roughly one wavelength and thus make it difficult to estimate the
19 wavelength directly from the 2D VTECP' map. So, the wavelength is derived from the
20 multiplication of speed and period.

21 However, those speed, period, and wavelength are the projections on longitudes. After adjusted by
22 the propagation azimuths that were calculated above, the final results of the estimated parameters
23 are listed in Table 1. It can be seen that these parameters show certain longitudinal dependence. It
24 should be noted that the data coverage is relatively lower in the east and west boundaries of the
25 investigated region. This may impact the accuracy of the estimation of the LSTID properties in
26 these areas. Besides, the mean values and standard deviations of the period, V_t , V_c , and
27 wavelength are 74.8 ± 1.4 minutes, 578 ± 16 m/s, 617 ± 23 m/s, and 2691 ± 80 km, respectively. These
28 parameters are typical for an LSTID. V_t and V_c overlap, although only marginally, considering the
29 error ranges. Meanwhile, the mean V_c is slightly larger than the mean V_t , which seems like the
30 wave behind is pushing that ahead. In general, the speed of trough and crest of the LSTID should
31 be rather the same since they are induced by the same gravity wave. However, the wave properties
32 might change with time dependent on the forcing from background condition, especially for
33 LSTID covering large spatial region. This might explain the differences.

34 In addition, it is interesting to note that V_t is in reasonable agreement with the result of 535 m/s
35 derived from the Doppler recordings. To show it more specifically, we estimated the speed and
36 direction of the LSTID using the same TLP method as Figure 8 but in 111°E-114°E and
37 29°N-38°N (corresponding to the reflecting points). The result is 562 ± 59 m/s and 0° , respectively.
38 In general, the LSTID velocity estimated from ground-based stations tend to be larger than the
39 actual velocity since these stations, in most cases, are not in perfect alignment with the
40 propagation direction of the LSTID [Afraimovich et al., 1998; Habarulema et al., 2013]. Such
41 good agreement between VTECP' and HF Doppler results may be attributed to the fact that the
42 reflecting points (29.2°N, 111.8°E; 38.0°N, 113.2°E) of the Doppler receivers are in a narrow
43 longitudinal band and the direction of the LSTID's propagation is also almost due south between

1 111°E-114°E.

2 As mentioned above, the VTECP' in the EIA region seems to exhibit different features compared
3 to that in the middle latitude. It can be seen from Figure 8(c) that VTECP' in this region also
4 shows a periodic variation, but it seems to have longer period and time duration than the LSTID.
5 These disturbances are probably related to the complex variations of VTEC after 08:00 UT
6 (around dusk). Besides, the perturbations at 20°N around 12:00 UT and 13:00 UT show patterns of
7 poleward movement. Habarulema et al. [2018] have identified TIDs in the Asian-Australian sector
8 during the same storm period. It provides clear examples of TIDs crossing the dip equator from
9 the southern hemisphere to the northern hemisphere around 09:00-12:00 UT. Their analysis shows
10 that these TIDs may not have exceeded 30°N. Such poleward feature is also detected in other
11 longitudinal sectors during this storm [Zakharenkova et al., 2016] and other storms [Pradipta et al.,
12 2016; Jonah et al., 2018]. In addition, Ding et al. [2013] have studied the poleward-propagating
13 LSTIDs in southern China during a medium-scale storm in 2011. They attribute their observations
14 to the excitation of secondary LSTIDs during the dissipation of primary disturbances from the
15 lower atmosphere. Besides, the poleward-moving disturbances may also be induced by the
16 variation of the equatorial electrojet as pointed out by Chimonas [1970] and more recently by
17 Habarulema et al. [2016]. A detailed investigation of this phenomenon is not the focus of this
18 work.

20 4. Discussion

21 Our results show that the propagation parameters of the LSTID in the East Asian sector during the
22 St. Patrick's Day storm are longitudinal dependent. Among these parameters, the longitudinal
23 dependence of the propagation azimuth of an LSTID receives much attention in previous works.
24 In general, earlier studies suggest that there are four main factors that affect the direction of a
25 polar originated LSTID, which are the velocity of the background neutral wind [Hines, 1960;
26 Morton and Essex, 1978; Maeda and Handa, 1980], the structure and evolution of the source
27 region in the auroral oval [Maeda and Handa, 1980; Hunsucker, 1982; Ding et al., 2007], the
28 Coriolis force [Maeda and Handa, 1980; Balthazor and Moffett, 1999; Afraimovich et al., 2000;
29 Tsugawa et al., 2004; Ding et al., 2013], and the declination of geomagnetic field [Tsugawa et al.,
30 2004; Borries et al., 2009].

31 The Coriolis force effect is generally believed to contribute to the clockwise shift of the
32 propagation direction of the LSTIDs [Afraimovich et al., 2000; Tsugawa et al., 2004; Ding et al.,
33 2013]. The observations of the shift (10°-20° on average) are consistent with the calculation by
34 Maeda and Handa [1980] and the model simulation by Balthazor and Moffett [1999]. However, in
35 our study, the shift of the propagation direction is not systematic westward, which means the
36 variability of the LSTID azimuth in our observation cannot be attributed to the Coriolis force, at
37 least not to it alone.

38 The structure/movement of the source region for the LSTID in the auroral oval is another
39 candidate for explaining the longitudinal dependence of the propagation direction of the LSTID.
40 Previous studies have suggested that the westward movement of enhanced electrojets in the
41 auroral arc is an important cause of the westward shift of the LSTID propagation direction at high

Section 3. **Marked-up Manuscript**

1 latitudes [Hunsucker, 1982; Ding et al., 2007]. The change of the propagation direction of LSTIDs
2 as they move from high to middle latitudes during the superstorm of 29 October 2003 over North
3 America, was explained by Ding et al. [2007] as related to a change in the position of the
4 electrojet enhancement area near the auroral oval. Nevertheless, since the structure and the
5 evolution process of the source region during storm period is complicated, more cases and
6 modeling studies are needed to find a clear connection between it and the propagation direction of
7 LSTIDs.

8 In general, the velocity of the neutral wind is much less than that of the LSTIDs, and the
9 thermospheric wind velocity in the same latitudinal belt with a limited longitudinal extension
10 should exhibit little variance. So, the contribution of the background wind on the change of the
11 propagating direction would be limited in the absence of the geomagnetic field. However, a
12 combined effect of magnetic declination and zonal wind can cause F region electron density
13 differences between two sides of the zero declination [Zhang et al., 2011]. During storm periods,
14 the enhanced zonal winds [Fuller-Rowell et al., 1994] can intensify these differences [Thomas et
15 al, 2016]. As a result, the geomagnetic declination is considered to be an important factor that
16 affects the propagation direction of the LSTID. Some researchers have studied the predominant
17 propagation direction of LSTIDs during storm periods in different longitudinal sectors, and
18 suggest that, statistically speaking, the predominant directions of LSTID in Europe, China and
19 Japan are primarily southward, South to West and South to East, respectively [Nicolls et al, 2004;
20 Tsugawa et al, 2004; Borries 2009; Ding et al, 2013]. These results are all consistent with the
21 corresponding geomagnetic declination in each sector.

22 In the longitudinal region of 70°E-150°E, the geomagnetic declination angles change from North
23 by East in the West side to North by West in the East side. This characteristic seems to show some
24 kind of consistent with the azimuth results in Table 1. To illustrate such connection quantitatively,
25 Figure 9 depicts the (a) the geomagnetic declination on the wavefront in different longitudes in
26 Figure 7 and (b) the propagation direction (azimuth-180°) of the LSTID at the same spot. The
27 connection between these two parameters is quite obvious in this event. This result manifests that
28 the propagation of LSTIDs in different longitudes is probably influenced by the orientation of the
29 geomagnetic field lines in the East Asian sector. In addition, the tendency of field-aligned
30 propagation of the LSTID indicates that it is driven by the neutral winds since the winds push the
31 plasma up and down along the magnetic field lines. **There is no evidence, such as simultaneous**
32 **perturbations at all latitudes in other cases [Borries et al., 2016; Zakharenkova et al., 2016], to**
33 **show that the LSTID in the Chinese/Japanese sector is affected by prompt penetration electric**
34 **field (PPEF) during the same period. Besides, considering the relatively low data coverage in the**
35 **East/West side of the studied region, it should be noted that our speculation needs to be verified**
36 **with more observational data and numerical simulation to reduce uncertainty in our propagation**
37 **estimation and to figure out the detailed physical processes.**

38 **During the 2015 St. Patrick's Day storm, LSTIDs in the European-African, American and**
39 **Asian-Australian sectors are detected and analysed with TEC observations [Borries et al., 2016;**
40 **Zakharenkova et al., 2016; Habarulema et al., 2018]. It shows clearly in their results that the**
41 **European sector also exhibits LSTIDs around 11:00 UT.** As a comparison, we also analysed these
42 LSTIDs but with VTEC data from the Madrigal database of the MIT Haystack Observatory. This
43 database has good spatiotemporal coverage for the European and American sectors. To derive the

Section 3. Marked-up Manuscript

1 VTECP, a narrow longitudinal band (10°E - 20°E , 30°N - 70°N) is first selected and the VTEC data
2 with the same latitude at the same time is average. At each latitude bin, the averaged VTEC forms
3 a time series and the temporal resolution is reset to 12 minutes (0.2 hours) with bin averaging.
4 Then, a running mean with a 1.5 hours window is conducted for each time series and their
5 difference is taken as the VTECP. The result is plotted in Figure 10 as a TLP. The fitting lines are
6 obtained with the same method as those in Figure 8.

7 Figure 10 is basically consistent with previous results, such as the synchronous perturbations
8 around 04:45 UT and 09:15 UT, and the LSTID structures between 10:00 UT and 17:00 UT.
9 Moreover, our result shows that the VTECP' behavior between 60°N and 70°N is quite different
10 from below. The pattern around 10:00 UT seems to represent a TID with smaller phase speed.
11 Considering the physical processes are more complex in such high latitudes [Foster et al., 2014],
12 we only focus on the perturbations below 60°N . The phase speeds estimated from the most distinct
13 crest and trough are $\sim 500\pm 51$ m/s and $\sim 427\pm 55$ m/s, respectively, and the estimated period is \sim
14 4.0 ± 0.2 hours. It is clear that the appearances of the LSTIDs are different in the European and the
15 East Asian sectors during the same UT period for the same storm event. Borries et al. [2016]
16 present a detailed study on the LSTID in Europe during this storm. It is suggested that the
17 perturbation occurring around 11:00 UT is special since it is impacted by PPEF and wind at the
18 same time. Comparatively, the LSTID in the Chinese/Japanese sector seems only driven by winds.
19 This may partly account for the longitudinal difference in our results. Besides, such difference
20 may also be related to the location or structure of the Joule heating source in the auroral oval or
21 the difference of the background TEC in the two sectors. For better understanding this difference,
22 more studies on the Joule heating source are needed.

23

24 5. Summary

25 Using data from 4 GPS receiver networks (CMGN, CMONOC, GEONET, IGS), together with
26 recordings of 2 HF Doppler shift stations and 8 ionosondes, we provide comprehensive and
27 detailed observation results of the LSTIDs in the East Asian sector during the 2015 St. Patrick's
28 Day storm. The GPS receiver networks in China and Japan are combined together to produce 2D
29 VTEC perturbation maps in order to give a wider image of the LSTID structures in the East Asia.
30 As a comparison, the ionospheric disturbances in the European sector are also studied with VTEC
31 data from the Madrigal database. The propagation parameters of the LSTIDs are estimated. Main
32 results can be summarized as follows:

33 (1) A trough of LSTID occurs and propagates from high to lower latitudes during 09:40-11:20 UT,
34 which spans over 60° in longitude. It is followed by a crest of LSTID that characterized by a clear
35 tendency to dissipate starting from the East side. These features are in good agreement with
36 observations by HF Doppler shift stations and ionosondes

37 (2) The propagation orientation is almost due southward around 105°E - 115°E , and it tends to
38 slightly shift westward/eastward in the West/East part of the studied area. This is expected to be
39 influenced by the regional declination of the geomagnetic field lines.

40 (3) The propagation parameters in different longitudinal bands are estimated. These parameters
41 show certain longitudinal differences. Besides, the mean values and standard deviations of the

Section 3. Marked-up Manuscript

1 period, V_t , V_c , and wavelength are 74.8 ± 1.4 minutes, 578 ± 16 m/s, 617 ± 23 m/s, and 2691 ± 80 km,
2 respectively.

3 It should be noted that our results show certain consistency with previous works focusing on the
4 Chinese or Japanese sector for different LSTID events. Nevertheless, the longitudinal dependence
5 shown in our results should be examined further with more case studies based on large
6 longitudinal and high-resolution coverage of GPS data.

7

8

9 **Acknowledgement:**

10 We are grateful to the International GPS Services (IGS) (<ftp://cddis.gsfc.nasa.gov>). The GPS data
11 from CMONOC and CMGN networks are provided by the China Earthquake Administration
12 (CEA) and the China Meteorological Administration (CMA), respectively. The GPS data from
13 GEONET are provided by the Geographical Survey Institute, Japan. GPS TEC data products and
14 access through the Madrigal distributed data system (<http://cedar.openmadrigal.org/>) are provided
15 to the community by the Massachusetts Institute of Technology under support from the US
16 National Science Foundation grant AGS-1242204. The HF Doppler records are from the Chinese
17 Meridian Project. The ionosonde data are provided by the China Research Institute of Radio wave
18 Propagation (CRIRP). We thank the NASA/GSFC's Space Physics Data Facility's OMNIWeb
19 service (<https://spdf.gsfc.nasa.gov>) for data of the interplanetary and SYM-H parameters. This
20 research was supported by the National Natural Science Foundation of China (No. 41674157).

21

22

23

References

- 1
2 Afraimovich, E. L., Palamartchouk, K. S., and Perevalova, N. P.: GPS radio interferometry of
3 travelling ionospheric disturbances. *Journal of Atmospheric and Solar-Terrestrial*
4 *Physics*, 60(12), 1205-1223, 1998.
- 5 Afraimovich, E. L., Kosogorov, E. A., Leonovich, L. A., Palamartchouk, K. S., Perevalova, N. P.,
6 and Pirog, O. M.: Determining parameters of large-scale traveling ionospheric disturbances
7 of auroral origin using GPS-arrays. *Journal of Atmospheric and Solar-Terrestrial*
8 *Physics*, 62(7), 553-565, 2000.
- 9 Astafyeva, E., Zakharenkova, I., and Förster, M.: Ionospheric response to the 2015 St. Patrick's
10 Day storm: A global multi-instrumental overview. *Journal of Geophysical Research: Space*
11 *Physics*, 120(10), 9023-9037, 2015.
- 12 Balthazor, R. L. and Moffett, R. J.: Morphology of large-scale traveling atmospheric disturbances
13 in the polar thermosphere. *Journal of Geophysical Research: Space Physics*, 104(A1),
14 15-24. Borries, C., Jakowski, N., & Wilken, V. (2009). Storm induced large scale TIDs
15 observed in GPS derived TEC. *Ann. Geophys*, 27(4), 1605-1612, 1999.
- 16 **Borries, C., Mahrous, A. M., Ellahouny, N. M., and Badeke, R.: Multiple ionospheric**
17 **perturbations during the Saint Patrick's Day storm 2015 in the European-African sector.**
18 ***Journal of Geophysical Research: Space Physics*, 121(11), 11-333, 2016.**
- 19 Borries, C., Jakowski, N., Kauristie, K., Amm, O., Mielich, J., and Kouba, D.: On the dynamics of
20 large-scale traveling ionospheric disturbances over Europe on 20 November 2003. *Journal of*
21 *Geophysical Research: Space Physics*, 122(1), 1199-1211, 2017.
- 22 Buonsanto, M. J.: Ionospheric storms—A review. *Space Science Reviews*, 88(3-4), 563-601,
23 1999.
- 24 Cherniak, I. and Zakharenkova, I.: Large-Scale Traveling Ionospheric Disturbances Origin and
25 Propagation: Case Study of the December 2015 Geomagnetic Storm. *Space Weather*, 16(9),
26 1377-1395, 2018.
- 27 Chimonas, G.: The equatorial electrojet as a source of long period travelling ionospheric
28 disturbances. *Planetary and Space Science*, 18(4), 583-589, 1970.
- 29 Coster, A. J. and Gaposchkin, E. M.: Use of GPS pseudo-range and phase data for measurement of
30 ionospheric and tropospheric refraction. In *Institute of Navigation Satellite Division, 2nd*
31 *International Technical Meeting* (pp. 439-443), 1989.
- 32 Ding, F., Wan, W., Ning, B., and Wang, M.: Large-scale traveling ionospheric disturbances
33 observed by GPS total electron content during the magnetic storm of 29-30 October
34 2003. *Journal of Geophysical Research: Space Physics*, 112(A6), 2007.
- 35 Ding, F., Wan, W., Liu, L., Afraimovich, E. L., Voeykov, S. V., and Perevalova, N. P.: A statistical
36 study of large-scale traveling ionospheric disturbances observed by GPS TEC during major
37 magnetic storms over the years 2003–2005. *Journal of Geophysical Research: Space*
38 *Physics*, 113(A3), 2008.
- 39 Ding, F., Wan, W., Ning, B., Zhao, B., Li, Q., Zhang, R., Xiong, B., and Song, Q.:
40 Two-dimensional imaging of large-scale traveling ionospheric disturbances over China based
41 on GPS data. *Journal of Geophysical Research: Space Physics*, 117(A8), 2012.
- 42 Ding, F., Wan, W., Ning, B., Zhao, B., Li, Q., Wang, Y., Hu, L., Zhang, R., and Xiong, B.:
43 Observations of poleward-propagating large-scale traveling ionospheric disturbances in
44 southern China. In *Annales Geophysicae* (Vol. 31, No. 2, p. 377). Copernicus GmbH, 2013.

Section 3. Marked-up Manuscript

- 1 Ding, F., Wan, W., Li, Q., Zhang, R., Song, Q., Ning, B., Liu, L., Zhao, B., and Xiong, B.:
2 Comparative climatological study of large-scale traveling ionospheric disturbances over
3 North America and China in 2011–2012. *Journal of Geophysical Research: Space*
4 *Physics*, 119(1), 519-529, 2014.
- 5 Figueiredo, C. A. O. B., Wrasse, C. M., Takahashi, H., Otsuka, Y., Shiokawa, K., and Barros, D.:
6 Large-scale traveling ionospheric disturbances observed by GPS dTEC maps over North and
7 South America on Saint Patrick's Day storm in 2015. *Journal of Geophysical Research: Space*
8 *Physics*, 122(4), 4755-4763, 2017.
- 9 Foster, J. C., Erickson, P. J., Coster, A. J., Thaller, S., Tao, J., Wygant, J. R., and Bonnell, J. W.:
10 Storm time observations of plasmasphere erosion flux in the magnetosphere and
11 ionosphere. *Geophysical Research Letters*, 41(3), 762-768, 2014.
- 12 Fuller-Rowell, T. J., Codrescu, M. V., Moffett, R. J., and Quegan, S.: Response of the
13 thermosphere and ionosphere to geomagnetic storms. *Journal of Geophysical Research:*
14 *Space Physics*, 99(A3), 3893-3914, 1994.
- 15 Habarulema, J. B., Katamzi, Z. T., and McKinnell L.-A.: Estimating the propagation
16 characteristics of largescale traveling ionospheric disturbances using ground-based and
17 satellite data, *J. Geophys. Res. Space Physics*, 118, 7768–7782, 2013.
- 18 Habarulema, J. B. and Carelse, S. A.: Long-term analysis between radio occultation and ionosonde
19 peak electron density and height during geomagnetic storms. *Geophysical Research Letters*,
20 43(9), 4106-4111, 2016.
- 21 Habarulema, J. B., Katamzi, Z. T., and Yizengaw, E.: First observations of poleward large-scale
22 traveling ionospheric disturbances over the African sector during geomagnetic storm
23 conditions. *Journal of Geophysical Research: Space Physics*, 120(8), 6914-6929, 2015.
- 24 Habarulema, J. B., Katamzi, Z. T., Yizengaw, E., Yamazaki, Y., and Seemala, G.: Simultaneous
25 storm time equatorward and poleward large-scale TIDs on a global scale. *Geophysical*
26 *Research Letters*, 43(13), 6678-6686, 2016.
- 27 Habarulema, J. B., Yizengaw, E., Katamzi-Joseph, Z. T., Moldwin, M. B., and Buchert, S.: Storm
28 Time Global Observations of Large-Scale TIDs From Ground-Based and In Situ Satellite
29 Measurements. *Journal of Geophysical Research: Space Physics*, 123(1), 711-724, 2018.
- 30 Hines, C. O.: Internal atmospheric gravity waves at ionospheric heights. *Canadian Journal of*
31 *Physics*, 38(11), 1441-1481, 1960.
- 32 Ho, C. M., Mannucci, A. J., Lindqwister, U. J., Pi, X., and Tsurutani, B. T.: Global ionosphere
33 perturbations monitored by the worldwide GPS network. *Geophysical Research*
34 *Letters*, 23(22), 3219-3222, 1996.
- 35 Hocke, K. and Schlegel, K.: A review of atmospheric gravity waves and travelling ionospheric
36 disturbances: 1982-1995. In *Annales Geophysicae* (Vol. 14, No. 9, p. 917), 1996.
- 37 Hunsucker, R. D.: Atmospheric gravity waves generated in the high-latitude ionosphere: A
38 review. *Reviews of Geophysics*, 20(2), 293-315, 1982.
- 39 Jonah, O. F., Coster, A., Zhang, S., Goncharenko, L., Erickson, P. J., Paula, E. R., and Kherani, E.
40 A.: TID observations and source analysis during the 2017 Memorial Day weekend
41 geomagnetic storm over North America. *Journal of Geophysical Research: Space Physics*,
42 123, 8749– 8765. <https://doi.org/10.1029/2018JA025367>, 2018.
- 43 Klausner, V., Fagundes, P. R., Sahai, Y., Wrasse, C. M., Pillat, V. G., and Becker-Guedes, F.:
44 Observations of GW/TID oscillations in the F2 layer at low latitude during high and low

Section 3. Marked-up Manuscript

- 1 solar activity, geomagnetic quiet and disturbed periods. *Journal of Geophysical Research: Space Physics*, 114(A2), 2009.
- 2
- 3 Klobuchar, J. A.: Design and characteristics of the GPS ionospheric time delay algorithm for
4 single frequency users. In *PLANS'86-Position Location and Navigation Symposium* (pp.
5 280-286), 1986.
- 6 Krankowski, A., Zakharenkova, I., Krypiak-Gregorczyk, A., Shagimuratov, I. I., and Wielgosz, P.:
7 Ionospheric electron density observed by FORMOSAT-3/COSMIC over the European region
8 and validated by ionosonde data. *Journal of Geodesy*, 85(12), 949-964, 2011.
- 9 Lanyi, G. E. and Roth, T.: A comparison of mapped and measured total ionospheric electron
10 content using global positioning system and beacon satellite observations. *Radio*
11 *Science*, 23(4), 483-492, 1988.
- 12 Lyons, L. R., Nishimura, Y., Zhang, S. R., Coster, A. J., Bhatt, A., Kendall, E., and Deng, Y.:
13 Identification of Auroral Zone Activity Driving Large-Scale Traveling Ionospheric
14 Disturbances. *Journal of Geophysical Research: Space Physics*, 124(1), 700-714, 2019.
- 15 Maeda, S. and Handa, S.: Transmission of large-scale TIDs in the ionospheric F2-region. *Journal*
16 *of Atmospheric and Terrestrial Physics*, 42(9-10), 853-859, 1980.
- 17 Mendillo, M. and Narvaez, C.: Ionospheric storms at geophysically-equivalent sites–Part 1:
18 Storm-time patterns for sub-auroral ionospheres. In *Annales Geophysicae* (Vol. 27, No. 4, pp.
19 1679-1694). Copernicus GmbH, 2009.
- 20 Morton, F. W. and Essex, E. A.: Gravity wave observations at a southern hemisphere mid-latitude
21 station using the total electron content technique. *Journal of Atmospheric and Terrestrial*
22 *Physics*, 40(10-11), 1113-1122, 1978.
- 23 Nicolls, M. J., Kelley, M. C., Coster, A. J., González, S. A., and Makela, J. J.: Imaging the
24 structure of a large-scale TID using ISR and TEC data. *Geophysical Research Letters*, 31(9),
25 2004.
- 26 Pederick, L. H., Cervera, M. A., and Harris, T. J.: Interpreting observations of large-scale traveling
27 ionospheric disturbances by ionospheric sounders. *Journal of Geophysical Research: Space*
28 *Physics*, 122(12), 2017.
- 29 Pradipta, R., Valladares, C. E., Carter, B. A., and Doherty, P. H.: Interhemispheric propagation and
30 interactions of auroral traveling ionospheric disturbances near the equator. *Journal of*
31 *Geophysical Research: Space Physics*, 121(3), 2462-2474, 2016.
- 32 Ramsingh, Sripathi, S., Sreekumar, S., Banola, S., Emperumal, K., Tiwari, P., and Kumar, B. S.:
33 Low-latitude ionosphere response to super geomagnetic storm of 17/18 March 2015: Results
34 from a chain of ground-based observations over Indian sector. *Journal of Geophysical*
35 *Research: Space Physics*, 120(12), 10-864, 2015.
- 36 Richmond, A. D. and Roble, R. G.: Dynamic effects of aurora-generated gravity waves on the
37 mid-latitude ionosphere. *Journal of Atmospheric and Terrestrial Physics*, 41(7-8), 841-852,
38 1979.
- 39 Rideout, W. and Coster, A.: Automated GPS processing for global total electron content data. *GPS*
40 *Solutions*, 10(3), 219-228, 2006.
- 41 Saito, A., Fukao, S., and Miyazaki, S.: High resolution mapping of TEC perturbations with the
42 GSI GPS network over Japan. *Geophysical research letters*, 25(16), 3079-3082, 1998.
- 43 Saito, A., Nishimura, M., Yamamoto, M., Fukao, S., Kubota, M., Shiokawa, K., Otsuka, Y.,
44 Tsugawa, T., Ogawa, T., Ishii, M., Sakanoi, and T., Miyazaki, S.: Traveling ionospheric

Section 3. Marked-up Manuscript

- 1 disturbances detected in the FRONT campaign. *Geophysical Research Letters*, 28(4),
2 689-692, 2001.
- 3 Shiokawa, K., Otsuka, Y., Ogawa, T., Balan, N., Igarashi, K., Ridley, A. J., Knipp, D. J., Saito, A.,
4 and Yumoto, K.: A large-scale traveling ionospheric disturbance during the magnetic storm of
5 15 September 1999. *Journal of Geophysical Research: Space Physics*, 107(A6), SIA-5, 2002.
- 6 Song, Q., Ding, F., Wan, W., Ning, B., Liu, L., Zhao, B., Li, Q., and Zhang, R.: Statistical study of
7 large-scale traveling ionospheric disturbances generated by the solar terminator over
8 China. *Journal of Geophysical Research: Space Physics*, 118(7), 4583-4593, 2013.
- 9 Thomas, E. G., Baker, J. B. H., Ruohoniemi, J. M., Coster, A. J., and Zhang, S. R.: The
10 geomagnetic storm time response of GPS total electron content in the North American
11 sector. *Journal of Geophysical Research: Space Physics*, 121(2), 1744-1759, 2016.
- 12 Tsugawa, T., Saito, A., Otsuka, Y., and Yamamoto, M.: Damping of large-scale traveling
13 ionospheric disturbances detected with GPS networks during the geomagnetic storm. *Journal*
14 *of Geophysical Research: Space Physics*, 108(A3), 2003.
- 15 Tsugawa, T., Saito, A., and Otsuka, Y.: A statistical study of large-scale traveling ionospheric
16 disturbances using the GPS network in Japan. *Journal of Geophysical Research: Space*
17 *Physics*, 109(A6), 2004.
- 18 Tsugawa, T., Shiokawa, K., Otsuka, Y., Ogawa, T., Saito, A., and Nishioka, M.: Geomagnetic
19 conjugate observations of large-scale traveling ionospheric disturbances using GPS networks
20 in Japan and Australia. *Journal of Geophysical Research: Space Physics*, 111(A2), 2006.
- 21 Wan, W., Ning, B., Yuan, H., Li, J., Li, L., and Liang, J.: TID observation using a short baseline
22 network of GPS receivers. *Acta Geodaetica et Geophysica Hungarica*, 32(3-4), 321-327,
23 1997.
- 24 Wang, C.: New Chains of Space Weather Monitoring Stations in China, *Space*
25 *Weather*, 8, S08001, doi:10.1029/2010SW000603, 2010.
- 26 Zakharenkova, I., Astafyeva, E., and Cherniak, I.: GPS and GLONASS observations of large-scale
27 traveling ionospheric disturbances during the 2015 St. Patrick's Day storm. *Journal of*
28 *Geophysical Research: Space Physics*, 121(12), 2016.
- 29 Zhang, D. H. and Xiao, Z.: Study of ionospheric response to the 4B flare on 28 October 2003
30 using International GPS Service network data. *Journal of Geophysical Research: Space*
31 *Physics*, 110(A3), 2005.
- 32 Zhang, D. H., Zhang, W., Li, Q., Shi, L. Q., Hao, Y. Q., and Xiao, Z.: Accuracy analysis of the
33 GPS instrumental bias estimated from observations in middle and low latitudes. In *Annales*
34 *Geophysicae* (Vol. 28, No. 8, pp. 1571-1580). Copernicus GmbH, 2010.
- 35 Zhang, S. R., Foster, J. C., Coster, A. J., and Erickson, P. J.: East-West Coast differences in total
36 electron content over the continental US. *Geophysical Research Letters*, 38(19), 2011.
- 37 Zhang, S. R., Erickson, P. J., Goncharenko, L. P., Coster, A. J., Rideout, W., and Vierinen, J.:
38 Ionospheric bow waves and perturbations induced by the 21 August 2017 solar
39 eclipse. *Geophysical Research Letters*, 44(24), 12-067, 2017.
- 40 Zhang, W., Zhang, D. H., and Xiao, Z.: The influence of geo-magnetic storms on the estimation of
41 GPS instrumental biases, *Ann. Geophys.*, 27, 1613-1623, doi:10.5194/angeo-27-1613-2009,
42 2009.
- 43

1 Captions of Table and Figures

2 **Table 1.** The estimated propagation parameters of the LSTID and the corresponding standard
 3 errors. The second column contains the propagation directions, which are measured clockwise
 4 from the South. V_t/V_c represents the phase speed estimated with certain wave trough/crest.

5 **Figure 1.** Locations of the GPS stations of different networks (colored dots), the HF Doppler shift
 6 stations (green stars), the National Time Service Center of China (grey stars), and the ionosondes
 7 (green triangles) that used in this study.

8 **Figure 2.** Temporal variations of (a) the solar wind speed (V_{sw}), (b) the IMF Bz component, (c)
 9 the SYM-H index, and (d) the AE index between 18:00 UT, 16 March 2015 and 06:00 UT, 18
 10 March 2015. The occurrence of SSC is shown with vertical dashed lines.

11 **Figure 3.** Temporal variations of the HF Doppler shift records from (a) MDT and (b) SZT
 12 between 08:00 UT and 14:00 UT, 17 March 2015.

13 **Figure 4.** A series of 2D VTECP' maps over the East Asian sector from the period of 09:40-09:50
 14 UT to 11:30-11:40 UT on 17 March 2015. The grey areas represent the nightside. The colorbar
 15 represents the VTECP' (units: TECu), which is transformed from the original VTECP value with
 16 equation (3) for a more viewer-friendly colormap. The green and yellow lines illustrate the least
 17 square fittings (order 2) for wavefronts.

18 **Figure 5.** Temporal variations of mean VTECP' near the Doppler reflection points between 08:00
 19 UT and 14:00 UT, 17 March 2015. Doppler shift recordings in Figure 3 are plotted with dashed
 20 lines for comparison.

21 **Figure 6.** Temporal variations of the virtual height for iso-frequency lines from 8 ionosondes
 22 between 08:00 UT and 12:00 UT, 17 March 2015. Frequencies are depicted on each iso-frequency
 23 line. The time resolution is 15 min for all stations. The black dashed lines indicate the downward
 24 phase change.

25 **Figure 7.** A detailed example of the wavefront fitting method. Green dots indicate the data points
 26 for least square fitting. Green arrows depict the propagation orientations in different longitudes.
 27 Dashed black rectangles mark the areas for generating TLPs in Figure 8.

28 **Figure 8.** TLPs of VTECP' for different longitudinal bands between 07:00-14:00 UT. White dots
 29 give the data points for linear fitting, and the fitting results are marked with white lines. 30°N in
 30 (b-d, f) is marked with black dashed lines which indicate the boundary of EIA. 40°N is marked in
 31 (f).

32 **Figure 9.** The sketch of (upper) the geomagnetic declination angels and (lower) the propagation
 33 directions in different longitudes on the wavefront fitted in Figure 7. The propagation directions
 34 are measured clockwise from the South.

35 **Figure 10.** The TLP of VTECP' for the European sector (10°E-20°E, 30°N-70°N) between
 36 01:00-23:00 UT. White lines and dots are similar to those in Figure 8. The black dashed line
 37 depicts 60°N.

38

Section 3. Marked-up Manuscript

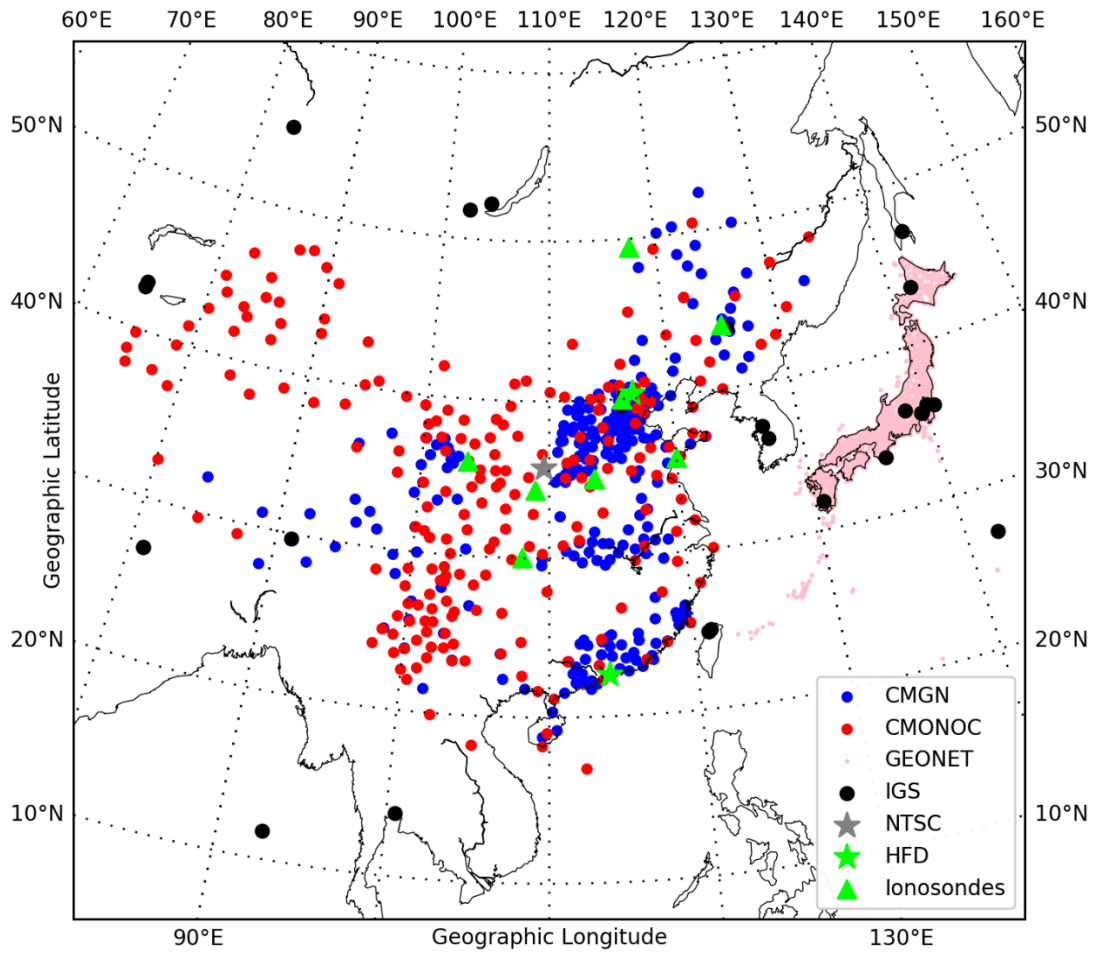
1 **Table 1.**

Lon. (°E)	Dir. (°)	Period (min)	Vt (m/s)	Vc (m/s)	Wavelength (km)
80-90	-11.2	81.1±3.4	500±40	542±31	2536±163
90-100	-7.1	77.6±5.2	552±22	670±44	2845±222
100-110	-2.9	58.8±1.5	587±47	638±76	2160±167
110-120	1.3	62.4±2.0	605±27	562±25	2184±99
120-130	7.9	94.2±1.3	647±39	673±63	3731±216

2

3

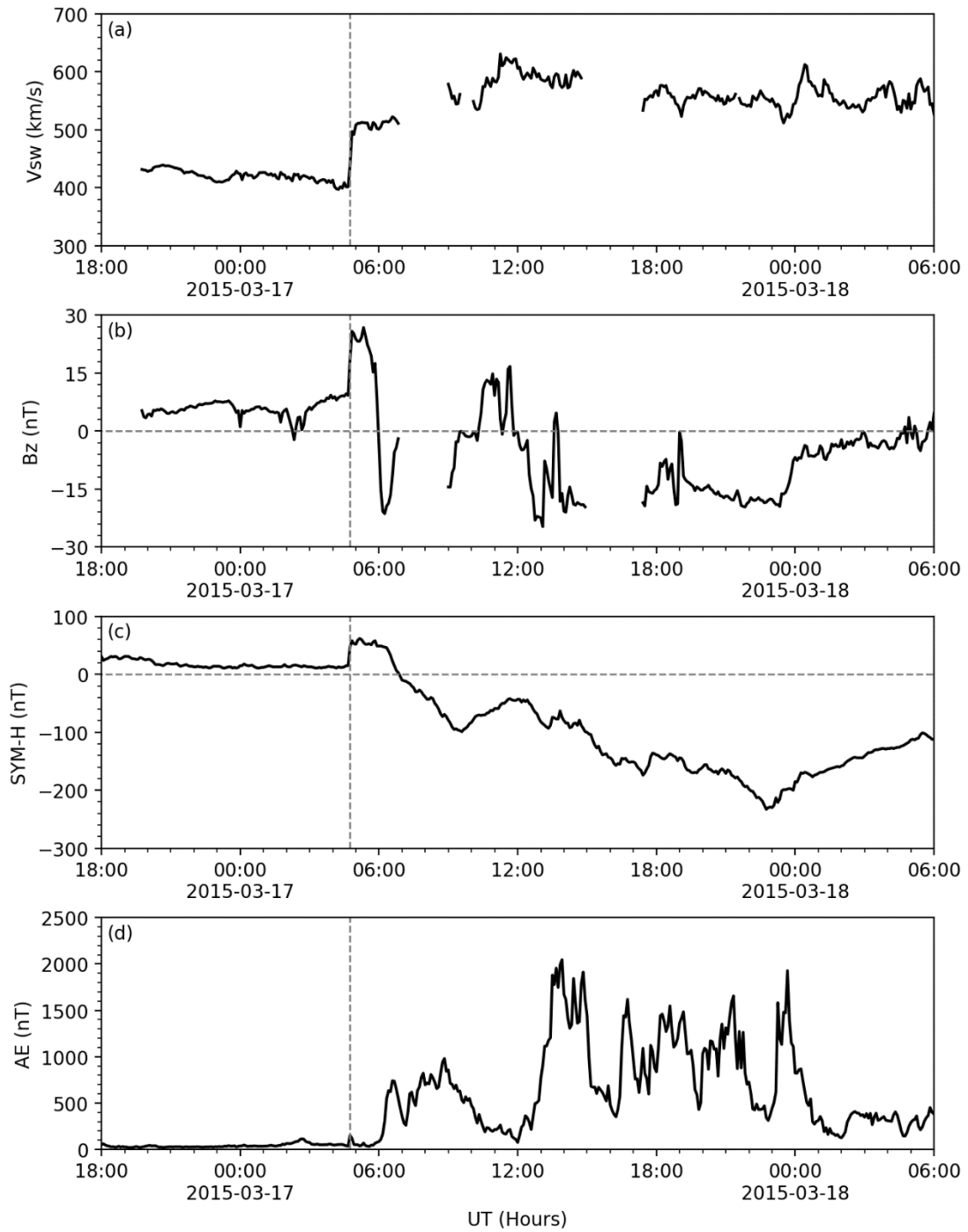
1 Figure 1.



2

3

1 Figure 2.

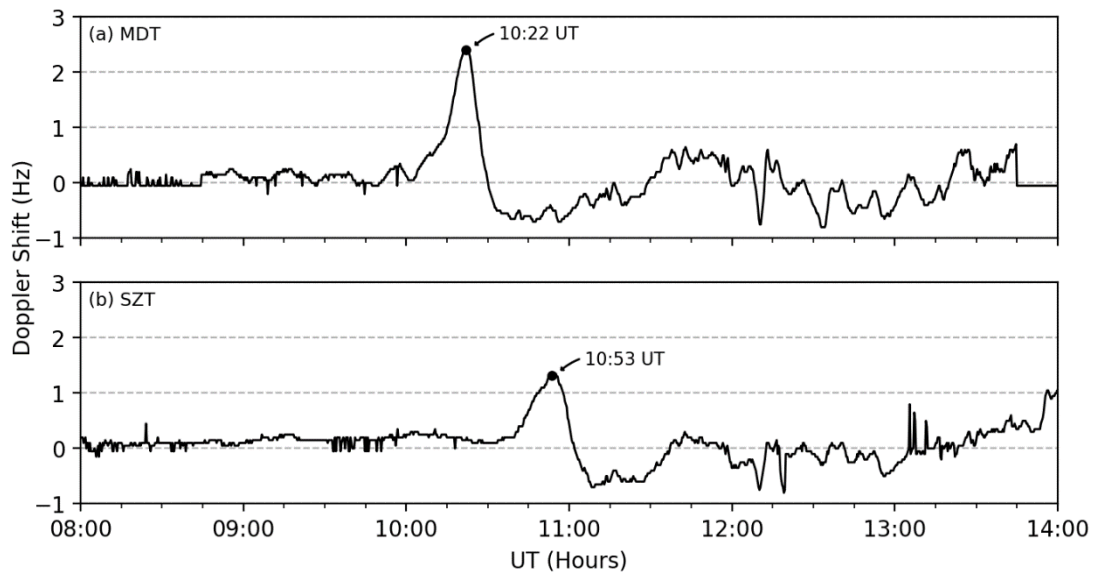


2

3

4

1 Figure 3.



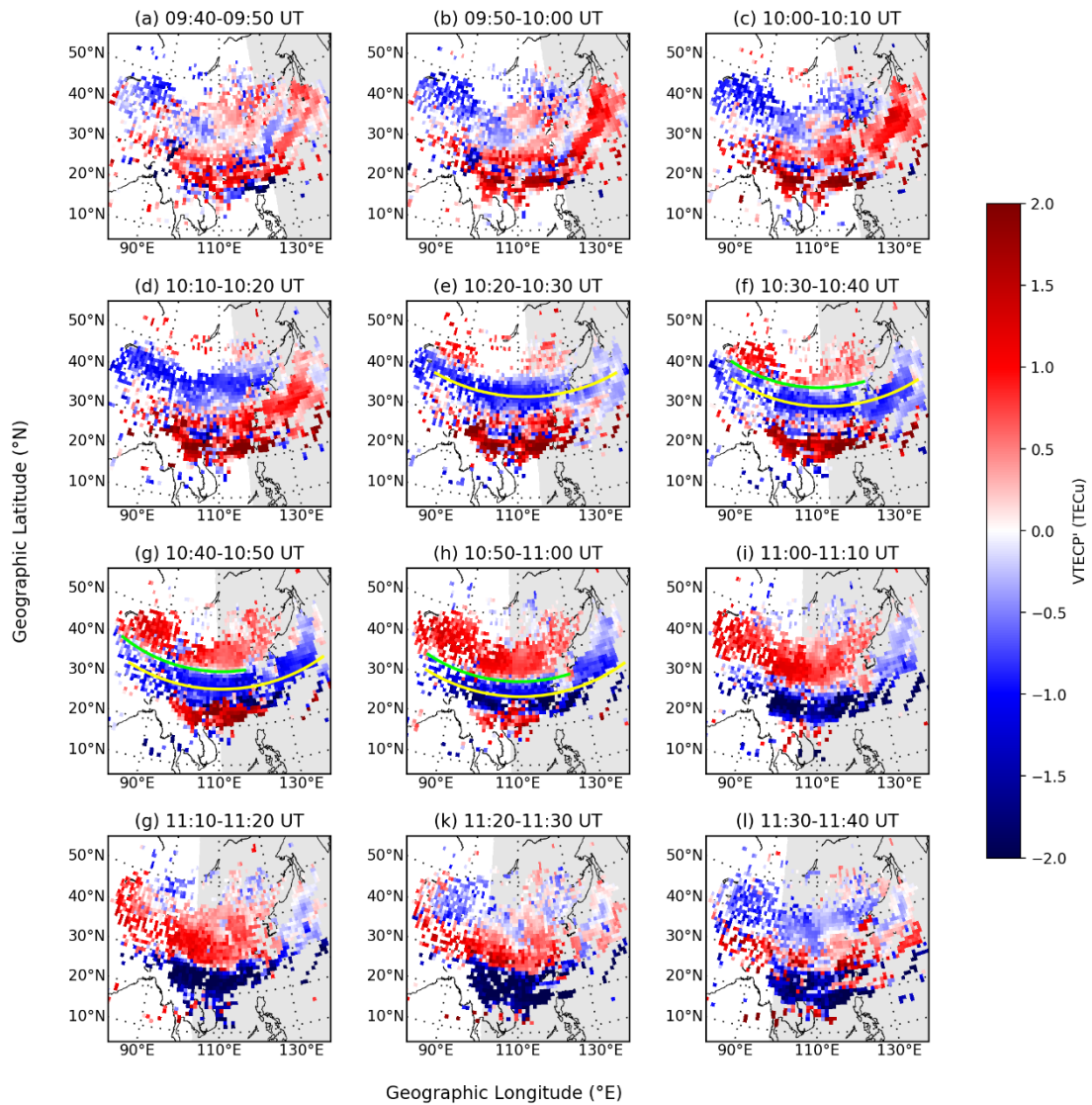
2

3

4

5

1 Figure 4.

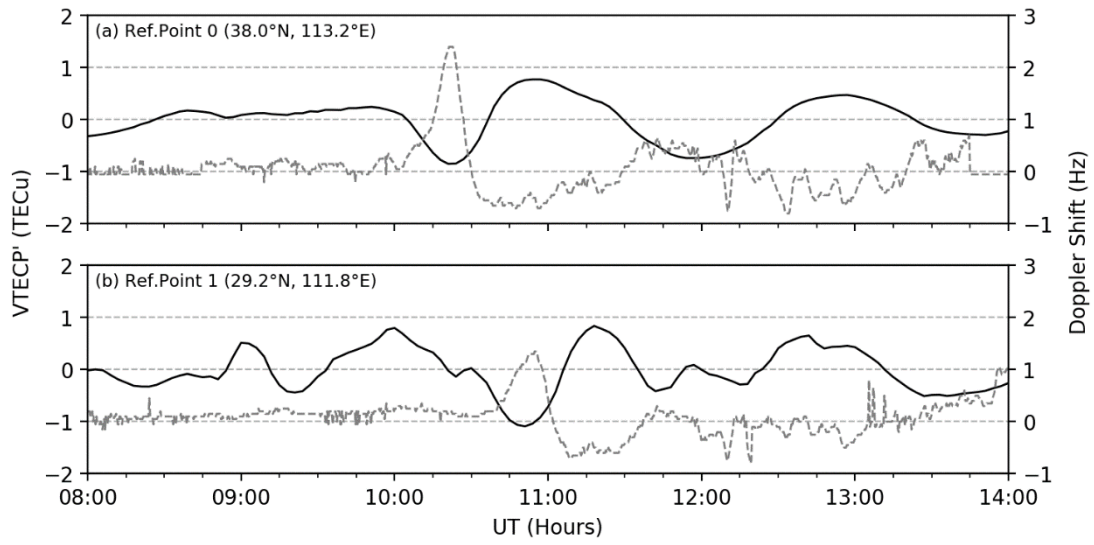


2

3

4

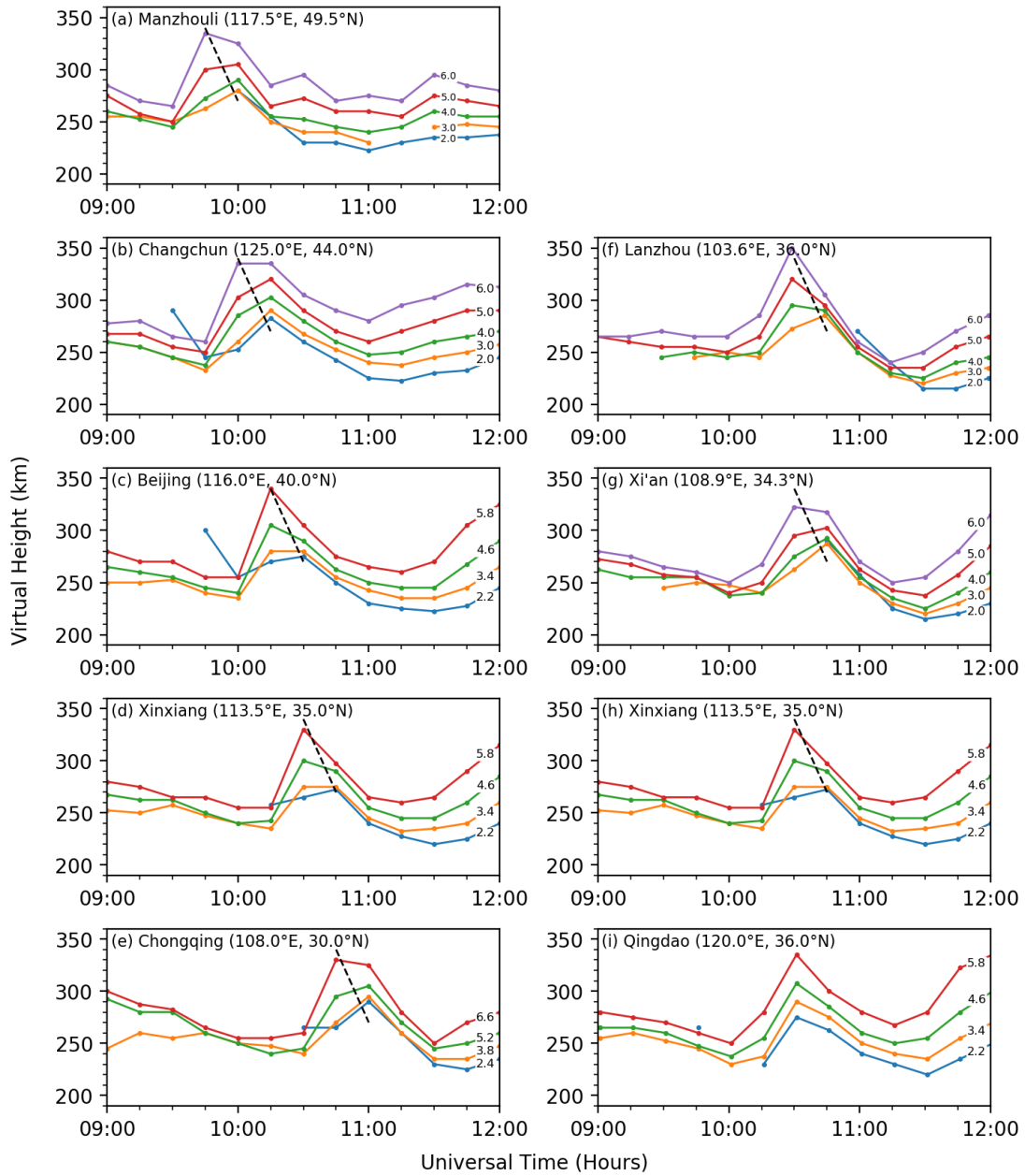
1 Figure 5.



2

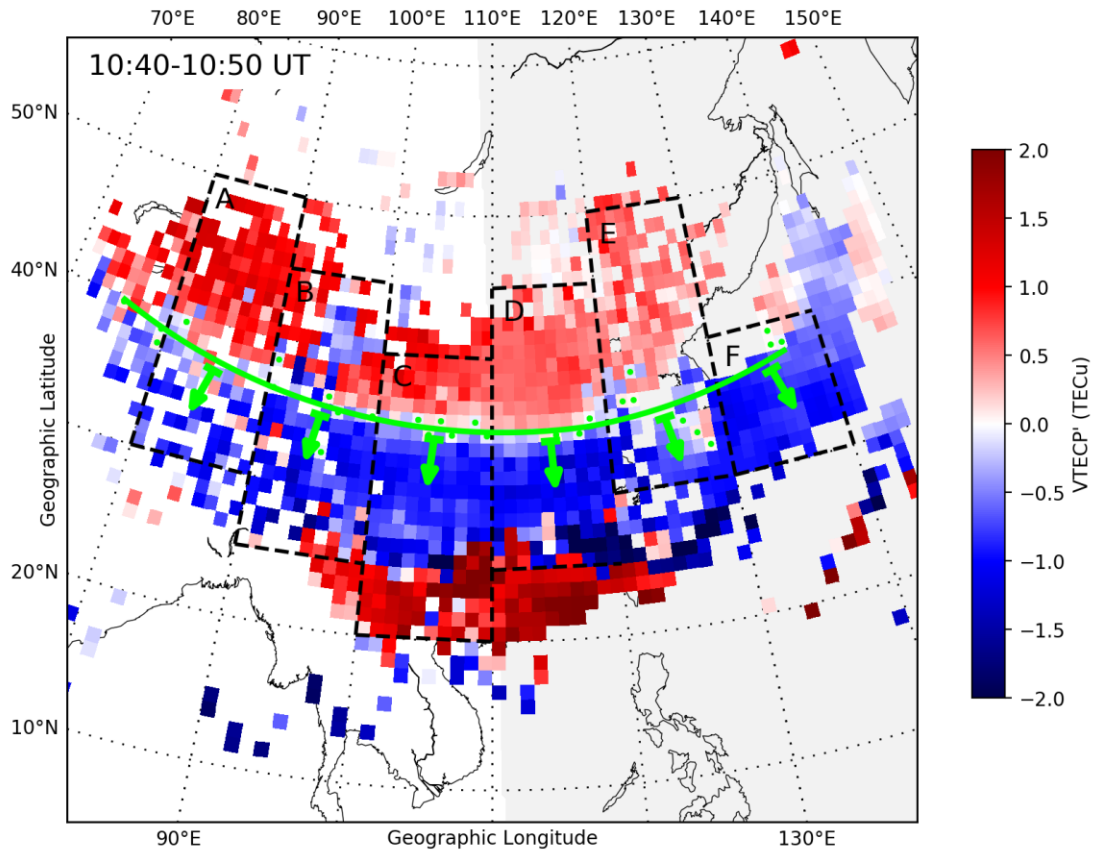
3

1 Figure 6.



2
3

1 Figure 7.



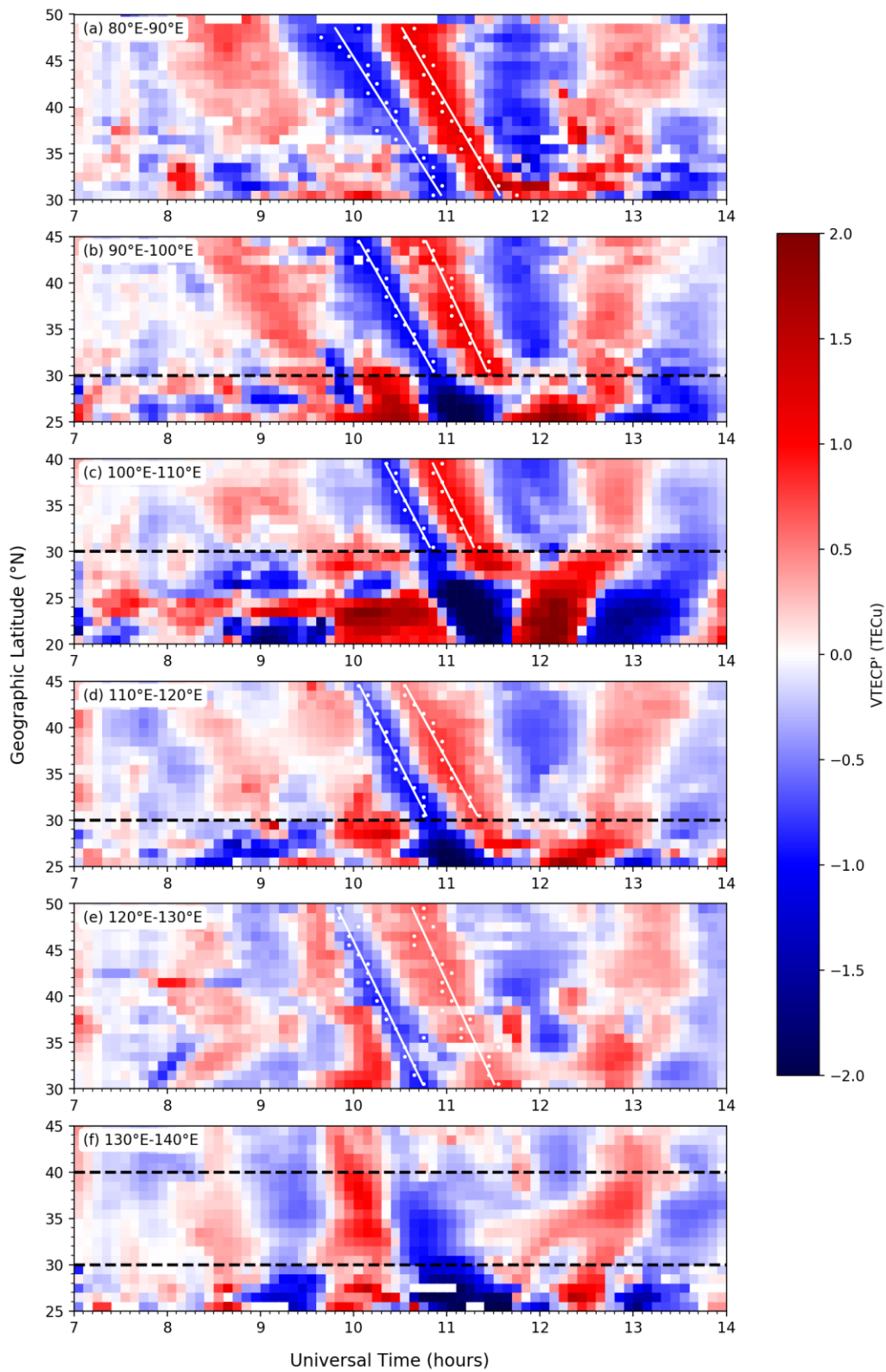
2

3

4

5

1 Figure 8.

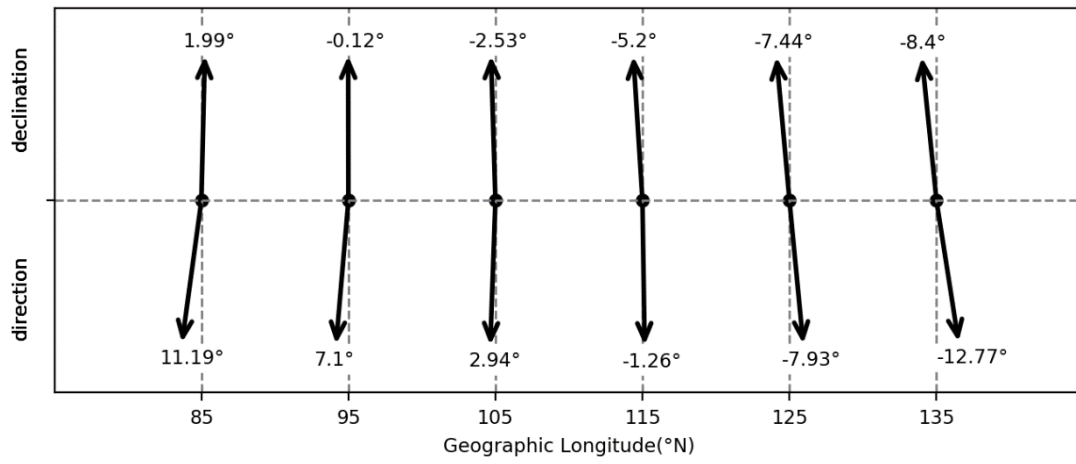


2

3

Section 3. Marked-up Manuscript

1 Figure 9.

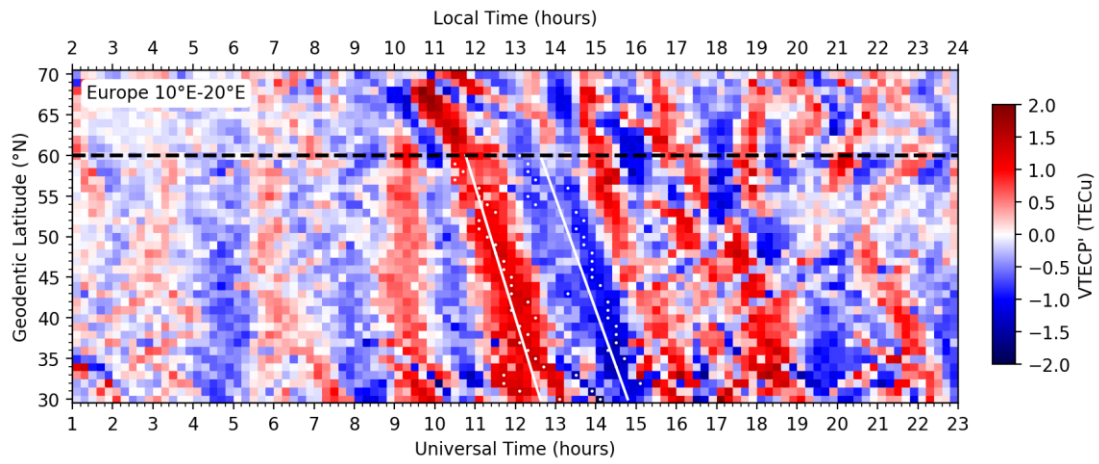


2

3

4

1 Figure 10.



2

3

4

5